Estuarine, Coastal and Shelf Science 212 (2018) 80–94

Contents lists available at ScienceDirect

Estuarine, Coastal and Shelf Science

journal homepage: www.elsevier.com/locate/ecss

Community composition and photophysiology of phytoplankton assemblages in coastal Oyashio waters of the western North Pacific during early spring

Kazuhiro Yoshida[a,*], Hisashi Endo[a,b,c], Evelyn Lawrenz[d], Tomonori Isada[e], Stanford B. Hooker[f], Ondřej Prášil[d], Koji Suzuki[a,b,**]

[a] Graduate School of Environmental Science, Hokkaido University, North 10 West 5, Kita-Ku, Sapporo, Hokkaido, 060-0810, Japan
[b] Faculty of Environmental Earth Science, Hokkaido University, North 10 West 5, Kita-Ku, Sapporo, Hokkaido, 060-0810, Japan
[c] Bioinformatics Center, Institute for Chemical Research, Kyoto University, Gokasho, Uji, Kyoto, 611-0011, Japan
[d] Laboratory of Photosynthesis, Institute of Microbiology, Czech Academy of Sciences, Opatovický mlýn, 37981, Třeboň, Czech Republic
[e] Akkeshi Marine Station, Field Science Center for Northern Biosphere, Hokkaido University, Aikkappu 1, Akkeshi-cho, Akkeshi-gun, Hokkaido, 088-1113, Japan
[f] Goddard Space Flight Center, National Aeronautical and Space Administration, 8880 Greenbelt Rd, Greenbelt, MD, 20771, USA

ARTICLE INFO

Keywords:
Coastal Oyashio
Spring diatom bloom
P-E curve
Diatom-specific *rbcL*
Chlorophyll *a* fluorescence

ABSTRACT

Globally, the western subarctic Pacific is known as the region with the largest seasonal drawdown in the partial pressure of CO_2 due to biological activity, i.e., high spring primary production and particulate organic carbon flux. These distinctive features are mainly caused by intense spring diatom blooms in coastal Oyashio (COY) and Oyashio (OY) waters. Although phytoplankton assemblages in OY waters are rather well studied, little is known about COY waters. In this study, photophysiological properties and phytoplankton community composition in COY waters were investigated during the pre-bloom and bloom periods from March to April 2015. Next-generation sequencing targeting the 18S rRNA gene revealed that the diatom *Thalassiosira* generally dominated the phytoplankton community and showed distinct differences in the diatom communities in shelf and offshore waters of the COY. Additionally, the relative contribution of *Thalassiosira* to the total diatom assemblages showed a positive correlation with maximum photosynthetic rates (P^B_{max}) occurring throughout this study. Chlorophyll *a* concentration and primary productivity were also positively correlated with sea surface temperature, suggesting that temperature was a critical factor for bloom development. Short-term on-deck incubation experiments were carried out to examine the role of temperature in determining planktonic photosynthetic processes. Our results showed an increase in P^B_{max} with rising temperature in assemblages from the shelf COY waters. Similarly, transcription levels of the diatom-specific *rbcL* gene, which encodes the large subunit of RuBisCO, also increased with rising temperature in the shelf assemblages. In contrast, temperature had little effect on the maximum photochemical quantum efficiency (F_v/F_m) of photosystem II. The results suggested that the transcription activity of the diatom-specific *rbcL* gene was upregulated by the increase in temperature, and that led to the higher P^B_{max} values and the spring diatom bloom in the shelf COY region.

1. Introduction

Photosynthetic marine phytoplankton are responsible for about half of the global primary production (Field et al., 1998; Behrenfeld et al., 2001) and are one of the principal drivers for the global carbon cycle (e.g. Sarmiento and Siegenthaler, 1992; Falkowski, 1994; Smetacek, 1999). The western subarctic Pacific has one of the highest transport efficiencies of particulate organic carbon (POC) in the water column (Honda, 2003; Kawakami et al., 2004, 2015) and the largest biological effect on seasonal changes in surface pCO_2 drawdown in the world ocean (Takahashi et al., 2002). These remarkable biogeochemical features are partly caused by large to vast spring diatom blooms observed in Oyashio (OY) and coastal Oyashio (COY) waters (Chiba et al., 2004; Hattori-Saito et al., 2010; Yoshie et al., 2010; Suzuki et al., 2011), which are biologically highly productive during spring (Isoda and Kishi, 2003; Isada et al., 2010). The OY is the westernmost current of the Western Subarctic Gyre (WSG) and is influenced by both the Eastern Kamchatka current and the Okhotsk Mode water (Yasuda, 2003; Oguma

* Corresponding author. Graduate School of Environmental Science, Hokkaido University, North 10 West 5, Kita-Ku, Sapporo, Hokkaido, 060-0810, Japan.
** Corresponding author. Graduate School of Environmental Science, Hokkaido University, North 10 West 5, Kita-Ku, Sapporo, Hokkaido, 060-0810, Japan.
E-mail addresses: kyoshida711@ees.hokudai.ac.jp (K. Yoshida), kojis@ees.hokudai.ac.jp (K. Suzuki).

https://doi.org/10.1016/j.ecss.2018.06.018
Received 20 October 2017; Received in revised form 8 May 2018; Accepted 16 June 2018
Available online 19 June 2018
0272-7714/

et al., 2008). The COY, on the other hand, is also derived from sea ice meltwater within the Sea of Okhotsk (Sugiura, 1956; Ohtani, 1971; Ogasawara, 1990) flowing along the southeastern coast of Hokkaido in spring (Kono, 1997; Kono et al., 2004; Oguma et al., 2008; Kusaka et al., 2013). Consequently, COY waters can generally be distinguished from the OY by their lower salinity (< 33) and lower temperature (– 1.8 to 2 °C) as the result of the sea ice meltwater in spring (Ohtani, 1971).

A number of studies have addressed the bloom dynamics in the OY region. For example, Suzuki et al. (2011) studied the community composition and bloom dynamics in OY waters and revealed that the annual spring bloom was often dominated by large, including chain-forming diatoms such as *Thalassiosira, Chaetoceros* and *Fragilariopsis* species. It was pointed out that development of steep density gradients in the water column (i.e., stratification) in spring can be associated with the initiation of the spring blooms in OY waters following the high nutrient supply into the surface mixed layer by winter deep mixing (Yoshimori et al., 1995; Kasai et al., 1997). Yoshie et al. (2003) noted that the deep mixing can significantly affect the amplitude of the spring OY bloom not only by the supply of nutrients but also by the dilution of predators, which drastically reduces grazing pressure (see Behrenfeld, 2010). Indeed, macrozooplankton grazing has a great impact on phytoplankton abundance, influencing the dynamics of the spring blooms in OY waters (Kasai et al., 1997; Saito et al., 2002; Kono and Sato, 2010). Saito et al. (2002) and Saito and Tsuda (2003) also proposed that light and silicate limitations could control the bloom dynamics in the OY region, particularly the initiation and termination of the spring diatom blooms. The spring diatom blooms in the OY waters can effectively foster the high productivity of higher trophic levels in this region (Taniguchi, 1999; Sakurai, 2007; Ikeda et al., 2008).

In contrast, fewer studies have been conducted in COY waters (Yoshimori et al., 1995; Kasai et al., 1997), even though the spring diatom blooms in COY waters have generally greater magnitude than those in OY waters (Isada et al., 2010; Okamoto et al., 2010) and contributes considerably to fisheries and aquaculture in this region (Nishimura et al., 2002; Isoda and Kishi, 2003). Like in OY waters, water column stratification may be highly relevant to the initiation of the bloom in COY waters (Kasai et al., 1997). Yoshimori et al. (1995) noted that the blooms in COY waters can exist for a longer time than those in OY waters due to continuous nutrient supply with its weaker vertical stability. The phytoplankton bloom in COY waters would significantly affect primary production in surrounding waters including the OY by physical processes such as advection and eddy diffusion (Shinada et al., 1999; Okamoto et al., 2010). These pilot studies on the spring blooms in COY waters investigated relationships among physical and biological parameters for estimating the bloom dynamics, but no study has been conducted to investigate the photophysiology and community composition of phytoplankton in COY waters. Low temperatures observed in COY waters can decrease growth rates and the photosynthesis of phytoplankton (Eppley, 1972; Raven and Geider, 1988). In addition, low temperatures in COY waters could be far below the thermal optimum for the carbon fixing enzyme of the Calvin cycle, Ribulose 1, 5- bisphosphate carboxylase/oxygenase (RuBisCO) (Descolas-Gros and de Billy, 1987; Young et al., 2015). In spite of low temperatures, however, intense and extensive diatom blooms are observed in COY waters every spring. Corresponding to the different origins of COY and OY waters, it can be expected that the composition of diatoms may also be distinct between these two water masses. Regarding zooplankton community, significant differences in community composition were reported at the species level between these water masses (Yamaguchi et al., 2003; Abe et al., 2014), however, information about possible differences in phytoplankton community composition are still missing.

From the aforementioned results, we hypothesized that (i) phytoplankton community composition in COY waters is distinctly different from offshore regions, and (ii) low temperatures in COY waters inhibit phytoplankton photosynthesis, specifically carbon fixation processes. In regards to the latter, we expect the subsequent warming of the water column during spring enhances photosynthetic activity. In this study, phytoplankton community composition in COY waters during spring was assessed with both phytoplankton pigment signatures and DNA-based next-generation sequencing (NGS) technology. Pigment analysis using the Suzuki et al. (2015) method of ultra-high performance liquid chromatography (UHPLC) allowed us to estimate the community composition of phytoplankton assemblages at the class level, whereas the relative contributions of each diatom genus to the total biomass of diatoms were quantified with the NGS method. In addition, the photophysiology of phytoplankton in COY waters during the pre-bloom and bloom periods were investigated using the following: a) active chlorophyll fluorescence techniques, e.g., pulse amplitude modulated (PAM) and fast repetition rate (FRR) fluorometry; b) the transcription activity of the diatom-specific *rbcL* gene, which encodes the large subunit of RuBisCO; c) carbon-based photosynthesis-irradiance (*P-E*) curve experiments; and d) 77 K emission spectroscopy. The active chlorophyll fluorescence techniques enabled us to measure photosynthetic activities (i.e., the maximum quantum yield of photochemistry) in photosystem II (hereafter PSII). On the other hand, transcription levels of the diatom-specific *rbcL* gene determined by reverse transcribed quantitative PCR can be used as an indicator for the activity of the light independent reactions of photosynthesis because RuBisCO encoded by the *rbcL* gene is the rate-determining enzyme of the process (John et al., 2007). Moreover, carbon-based *P-E* curves provide powerful insights into photophysiological states such as photoacclimation and nutrient stress (Sakshaug et al., 1997; MacIntyre et al., 2002) through the whole photosynthetic processes from light absorption to carbon fixation. Emission spectroscopy also provided semiquantitative information about the presence of major taxonomic groups and the physiological status of phytoplankton. The combination of these techniques provides us with holistic information on the photosynthetic processes of phytoplankton in COY waters. To elucidate the photophysiological responses of phytoplankton to temperature, we also performed, for the first time ever, temperature-controlled bottle incubation experiments in COY waters.

2. Materials and methods

2.1. Water sampling and optical observation

Seawater samples were collected from the western subarctic Pacific off the southeastern Hokkaido (Japan) coast as part of the R/V *Hakuho Maru* KH15-1 expedition during 6–26 March 2015 and the TR/V *Misago Maru* field study (hereafter AK15 expedition) during 16–17 April (Fig. 1). Prior to water sampling during the KH15-1 expedition, vertical profiles of photosynthetically available radiation (PAR) spanning 400–700 nm, E_d(PAR) and spectral downward irradiance, $E_d(\lambda)$, were obtained with the Compact-Optical Profiling System (C-OPS) co-developed by Biospherical Instruments Inc. and NASA (Hooker et al., 2013). Vertical attenuation coefficients of downward PAR, K_d (PAR) were determined as the slopes of a least-squares regression of the natural-log transformed E_d(PAR) profiles using Processing of Radiometric Observation of Seawater using Information Technologies (PROSIT) software (Hooker, 2014). Based on the derived K_d (PAR) value, euphotic zone depth (Z_{eu}) was calculated as the depth with 1% of the surface PAR remaining (Kirk, 2010). The incident PAR above the sea surface (E_0) was measured on-deck continuously with an LI-190SB air quantum PAR sensor and recorded by a LI-1400 data logger (LI-COR, Inc.) every 5–10 min. Surface (~5 m depth) seawater samples were obtained using a CTD carousel multi-sampler system (CTD-CMS) with acid-cleaned Niskin bottles. Upon collection, seawater was poured into a 9 L polycarbonate (PC) carboy, four 300 mL PC bottles for the measurements of primary productivity, and two polystyrene tubes for nutrient analyses. Concentrations of nutrients (nitrate + nitrite, ammonia, phosphate, and silicate) were determined with a BRAN-LUEBEE

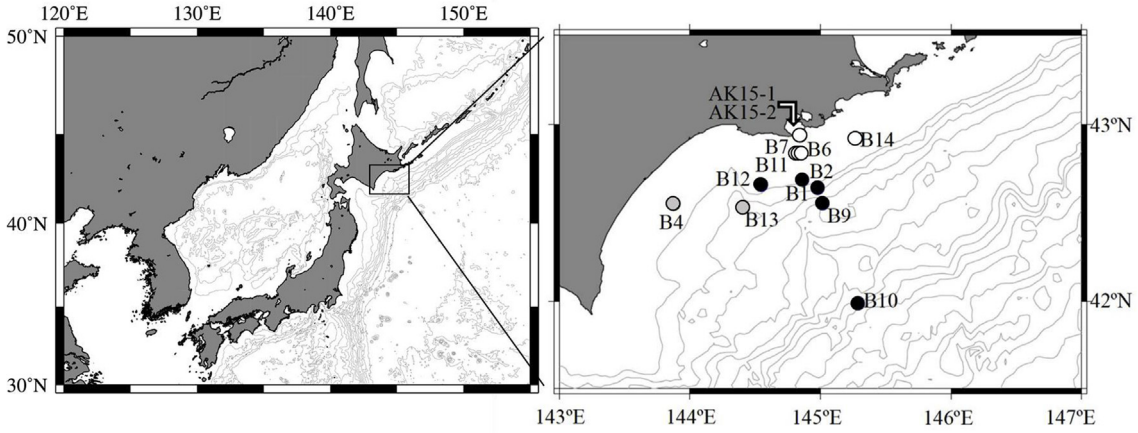

Fig. 1. Seawater sampling stations during the KH15-1 and AK15 expeditions off the coast of Hokkaido, Japan. Stations for the KH15-1 expedition are denoted as B plus station numbers. Stations Bio-6, Bio-7, and Bio-11 overlap as well as stations AK15-1 and AK15-2. Open circles denote shelf COY stations, black closed circles denote offshore COY stations, and grey closed circles denote Tokachi stations.

autoanalyzer (QuAAtro). Mixed layer depths (MLD) at all stations were calculated as the depth at which the potential density anomaly ($\Delta\sigma_\theta$) of the water column increased by 0.125 kg m^{-3} relative to the layer at 10 m (Monterey and Levitus, 1997).

2.2. Phytoplankton pigment composition

Seawater was dispensed into two 1 L PC bottles and these subsamples were filtered onto GF/F filters using a gentle vacuum (< 0.013 MPa). Filters were then blotted dry between filter papers, placed into cryovials, and immediately frozen in liquid nitrogen. Frozen filters were stored at −80 °C until further analysis. Pigments were extracted with the *N*, *N*-dimethylformamide (DMF) sonication method of Suzuki et al. (2002). Pigment concentrations were then determined by high-performance liquid chromatography (HPLC) or UHPLC following Van Heukelem and Thomas (2001) with a few modifications and Suzuki et al. (2015), respectively. To estimate phytoplankton community composition at the class level, multiple linear regression analyses based on major diagnostic pigment signatures and chlorophyll *a* (Chl *a*) were performed following Suzuki et al. (1997) and Obayashi et al. (2001), wherein fucoxanthin (Fuco) and peridinin (Peri) are representative algal marker pigment for diatoms and dinoflagellates, respectively. Although Fuco can also be observed in other phytoplankton taxa, e.g., chrysophytes, haptophytes and some dinoflagellates, we assumed Fuco was solely derived from diatoms in this study. This assumption can be justified with the results of Suzuki et al. (2011) who found a significant relationship between Fuco and diatom carbon during a spring bloom study in the study area. The following multiple linear regression of pigment markers was used:

$$[\text{Chl } a] = A[\text{Fuco}] + B[\text{Peri}] + C, \quad (1)$$

wherein [Chl *a*], [Fuco], and [Peri] are the concentrations of each pigment; *A* and *B* are partial regression coefficients for each concentration of the pigment markers; and *C* is a constant term of the multiple linear regression. The multiple linear regression analysis, and its validation with a *t*-test for each coefficient plus *F*-test, were performed with SigmaPlot software program ver. 11.0 (System Software). After this procedure, the contributions of each phytoplankton taxon to the total Chl *a* level were calculated by dividing a product of each concentration of pigment and its coefficient value by [Chl *a*] for each station.

2.3. Size-fractioned Chl a concentration

Seawater samples were filtered onto a 47 mm nylon mesh (20 μm pore size), a 47 mm Nuclepore membrane (10 or 2 μm pore size) and a 25 mm Whatman GF/F filter (nominal pore size 0.7 μm) using a gentle vacuum (< 0.013 MPa). After filtration, filters were placed in cryovials, immediately flash frozen in liquid nitrogen, and stored at −80 °C until further analysis. After thawing, the filters were transferred into glass cuvettes and soaked in 6 mL DMF at −20 °C for at least 24 h to extract phytoplankton pigments (Suzuki and Ishimaru, 1990). Chl *a* concentrations were determined with a Turner Designs 10-AU fluorometer using the non-acidification method of Welschmeyer (1994). The three size classes were defined as microphytoplankton (> 20 μm), nanophytoplankton (2–20 μm), and picophytoplankton (0.7–2 μm).

2.4. Ion Torrent next-generation sequencing (NGS)

Seawater samples for DNA analysis were collected sequentially on 25 mm polycarbonate Isopore filters (Millipore, 2 μm pore size) with a gentle vacuum (< 0.013 MPa) and then stored at −80 °C until further analysis. DNA samples were extracted using the method of Endo et al. (2013). Extracted DNA samples were purified using a NucleoSpin® gDNA Clean-up (Macherey-Nagel) following the manufacturer's protocols. The extracted DNA was sequenced with an Ion Torrent Personal Genome Machine (PGM) targeting the diatom-specific 18S rRNA gene V4 region. NGS libraries of DNA were constructed for each sample obtained from all stations and from the temperature-controlled incubation experiments. Gene fragments of the diatom-specific 18S rRNA V4 region sequences were amplified with the Takara Ex Taq Hot Start Version (Takara) and diatom-specific fusion primer pairs with 12 barcodes:

Forward primer: 5′-GATGATGARAAYATTAACTCW-3′

Reverse primer: 5′-TAWGAACCTTTWACTTCWCC-3′

The forward primer included the A-adapter sequence (5′-CCATCT CATCCCTGCGTGTCTCCGAC-3′), the key sequence (5′-TCAG-3′), the barcode sequences set by the manufacturer (Thermo Fisher Scientific) and a barcode adapter sequence (5′-GAT-3′) upstream of the forward primer. The reverse primer included the truncated Pi-adapter (trP1: 5′-CCTCTCTATGGGCAGTCGGTGAT-3′) sequence upstream of the reverse primer. PCR mixtures consisted of 1 × Ex Taq Buffer, 0.2 mM dNTP, 0.4 μM of the fusion primers, 0.625 unit of Taq polymerase, and 2 μL DNA template for a 25 μL total volume. PCR cycles within a thermal cycler were performed using the following conditions: 94 °C for 60 s, 30 cycles under 98 °C for 10 s, 56 °C for 30 s, and 72 °C for 60 s. After the final cycle, the temperature was held at 72 °C for 10 min to complete the PCR reactions. PCR products were purified with an Agencourt AMPure XP Kit (Beckman Coulter) and 70% ethanol following the manufacturer's protocols. The concentration of the purified

amplicons was determined with an Agilent 2100 Bioanalyzer (Agilent Technologies) using an Agilent 1000 Assay Kit according to the manufacturer's protocol. Based on the results of the Bioanalyzer, the purified amplicons were diluted to a concentration of 13 pM. Once NGS libraries were constructed, emulsion PCR was conducted with an Ion One Touch 2 system and an Ion PGM Template OT2 400 kit (Thermo Fisher Scientific). The resultant emulsion PCR products were then enriched with Ion One Touch ES (Thermo Fisher Scientific) according to the manufacturer's protocols. The enriched templates were loaded onto an Ion 318 v2 chip (Thermo Fisher Scientific) and amplicon libraries were sequenced with an Ion Torrent PGM system using the Ion PGM sequencing 400 kit v2 (Thermo Fisher Scientific) following the manufacturer's protocols.

To remove sequences with low quality and polyclonal sequences which did not match the A-adapter, quality filtering was initially performed with the Torrent Suite™ Software (Thermo Fisher Scientific). Additionally, inapplicable sequencing reads which unmatched the trP1 adapter sequence and the reverse primer sequence were removed with the FASTX-Toolkit (http://hannonlab.cshl.edu/fastx_toolkit/). After removal of forward and reverse primers, reads between 18 and 270 bp were extracted as 18S rRNA V4 regions. In addition, reads with a quality score of less than 23 were also excluded from the analysis. The obtained sequences were exported as FASTQ files and then converted to FASTA files with the mothur v. 1.25.0 (Schloss et al., 2009) software.

Using the FASTA files obtained for taxonomic classification based on the diatom-specific 18S rRNA V4 region, representative 10,000 reads were deposited to the SILVAngs web interface (https://www.arb-silva.de). The reads were classified with >93% classification similarity to SILVA SSU Ref dataset 123.1. Data which did not match diatoms were excluded from the classification results. For full details of the sequencing methods, see Endo et al. (2016).

2.5. Variable Chl a fluorescence by PAM and FRR fluorometry

Seawater was dispensed in a 30 mL amber bottle and stored in the dark at ambient temperature for 30 min for dark acclimation to ensure fully open PSII reaction centers. After acclimation, samples were transferred to a quartz cuvette (15 mm pathlength) in a dark environment and placed inside a pulse amplitude modulation (PAM) fluorometer (Walz, Germany) and a fast repetition rate (FRR) fluorometer (Chelsea Technologies Group, West Mosley, UK) to determine the maximum quantum yield of photochemistry in PSII defined as F_v/F_{mPAM} and F_v/F_{mFRRf} for measurements made with the PAM and FRR fluorometers, respectively. In addition to F_v/F_{mFRRf}, the FRRf also provided measurements of the effective absorption cross sections of PSII, σ_{PSII}, and the concentration of functional PSII reaction centers, [RCII]. PAM and FRR fluorometry measurements were conducted on multiple subsamples from each sample (i.e., pseudo-replication) following Liu et al. (2009) for PAM fluorometry, and Kolber et al. (1998) and Oxborough et al. (2012) for FRRf fluorometry.

2.6. Light absorption coefficient of phytoplankton

Seawater was filtered onto Whatman GF/F filters using a gentle vacuum (<0.013 MPa). After filtration, filters were carefully wrapped in aluminum foil to avoid any creases and then stored at −80 °C until further analysis. Following Kishino et al. (1985), the optical density of particles and detritus on the filters (OD_{fp} and OD_{fd}, respectively) was measured with a multipurpose scanning spectrophotometer (MPS-2450, Shimadzu) equipped with an end-on type photomultiplier tube in 1 nm steps from 350 to 800 nm before and after soaking filters in methanol for 15 min to remove phytoplankton pigments. Measurements before methanol extraction corresponded to the total absorption, those after methanol extraction to OD_{fd} and the difference between the two to OD_{fp}. All spectra were scatter corrected by subtracting the average value from 730 nm to 750 nm across the visible range (Babin and Stramski, 2002). Both OD_{fp} and OD_{fd} were converted to absorption coefficients, $a_p(\lambda)$ and $a_d(\lambda)$, respectively, using an appropriate path length amplification factor (Cleveland and Weidemann, 1993). The resultant $a_p(\lambda)$ values were then averaged from 400 to 700 nm and weighted to the spectral irradiance of the incubator lamp, $E_{PARinc}(\lambda)$ used for photosynthesis versus irradiance measurements to give mean absorption coefficients of phytoplankton ($\bar{a}_{ph}$) and mean Chl *a*-specific absorption coefficient of phytoplankton, $\bar{a}^*_{ph}$ following Isada et al. (2013).

2.7. Photosynthesis vs. irradiance (P-E) curves and photosynthetic parameters

For each curve, seawater samples were dispensed into twelve 275 mL polystyrene bottles and inoculated with ca. 0.1 mg of $NaH^{13}CO_3$ (99 atom% ^{13}C purity, Cambridge Isotope Laboratories, Inc.). Two bottles at time zero remained without any isotope. Samples were then incubated in a temperature-controlled incubator under 10 different light intensities between 1.44 and 1800 µmol photons m^{-2} s^{-1} for 2 h under both, ambient or an altered temperature (see details below under point 2.9). After incubation, samples were filtered onto pre-combusted 25 mm GF/F glass fiber filters (Whatman), which were stored at −80 °C until further analysis. Photosynthetic rates were calculated from ^{13}C uptake rates measured with an on-line element analyzer (FlashEA1112, Thermo Finnigan)/isotope ratio mass spectrometer (Delta-V, Thermo Finnigan) (EA/IRMS) following Hama et al. (1983), normalized to Chl *a* and plotted versus irradiance. The resultant P^B-*E* curves were fitted to the model of Platt et al. (1980):

$$P^B = P^B_s\left[1 - \exp\left(-\alpha^B.\frac{E_{PAR\ inc}}{P^B_s}\right)\right]\cdot\exp\left(-\beta^B.\frac{E_{PAR\ inc}}{P^B_s}\right),\ \text{and}\ P^B_{max} = P^B_s.[\alpha^B/(\alpha^B+\beta^B)]\cdot[\beta^B/(\alpha^B+\beta^B)]^{(\beta^B/\alpha^B)} \quad (2)$$

where, the superscript B denotes the biomass parameter used for normalization (here Chl *a*): P^B_{max} [mg C mg Chl a^{-1} h^{-1}] is the maximum photosynthetic rate; α^B [(mg C mg Chl a^{-1} h^{-1}) (µmol photons m^{-2} $s^{-1})^{-1}$] is the initial slope of the curve, or light utilization efficiency; $E_{PAR\ inc}$ [µmol photons m^{-2} s^{-1}] is the PAR at each bottle in the incubator; β^B [(mg C mg Chl a^{-1} h^{-1}) (µmol photons m^{-2} $s^{-1})^{-1}$] is the photoinhibition index; and P^B_s the maximum photosynthetic rate in the absence of photoinhibition. The light saturation index, E_k [µmol photons m^{-2} s^{-1}] was calculated as $E_k = P^B_{max}/\alpha^B$ and the maximum quantum yield for carbon fixation, Φ_{Cmax} [mol C mol photons^{-1}] was also calculated as:

$$\Phi_{Cmax} = 0.0231\alpha^B/\bar{a}^*_{ph}, \quad (3)$$

with further details provided by Isada et al. (2013).

2.8. Primary productivity

Seawater was dispensed into four acid-cleaned 300 mL PC bottles, inoculated with ~0.1 mg of $NaH^{13}CO_3$ and incubated for 24 h in an on-deck incubator at ambient temperature, either at ambient irradiance (3 replicate samples) or in darkness (1 sample). After incubation, samples were filtered onto pre-combusted 25 mm GF/F glass fiber filters (Whatman) and stored at −80 °C until further analysis as described above. Primary productivity, *PP* in the units of mg C m^{-3} day^{-1} for each sample was then calculated following Hama et al. (1983).

2.9. Temperature-controlled incubation experiments

To assess the effects of temperature on phytoplankton assemblages in COY waters, on-deck temperature-controlled bottle incubation experiments were conducted using surface seawater collected from ca. 5 m depth, and dispensed into three 9 L PC carboys at stations Bio-6, Bio-7, Bio-10, and Bio-13 (Fig. 1). One of the three carboys was used for

time zero samples, the remaining two were used to test for the effect of temperature, with ambient temperature being the control and +7 °C being the high temperature treatment. To avoid any interference from possible light effects, bottles were covered with black foil during the entire 24 h incubation. After incubation subsamples were collected to determine diatom community composition by NGS (Section 2.4) and to measure photosynthetic physiology by variable fluorescence and *P-E* experiments (Sections 2.5 and 2.7) combined with analyses of the transcription level of the diatom-specific *rbcL* gene by qRT-PCR(see following).

2.10. Transcription level of diatom-specific rbcL with qRT-PCR method

Sampling and extraction of DNA were performed as described above (Section 2.4). Seawater for RNA samples was filtered onto 25 mm polycarbonate Isopore filters (Millipore, 2 μm pore size) with a gentle vacuum (< 0.013 MPa). Filters for RNA analysis were placed in cryotubes containing 0.2 g of pre-combusted 0.1 mm glass beads and 600 μL RLT buffer (Qiagen), to which 10 μL β-mercaptoethanol (Sigma-Aldrich) were added. After filtration, RNA samples were immediately frozen in liquid nitrogen and stored at −80 °C until further analysis. RNA retained on the filters were extracted following Endo et al. (2015). The extracted RNA was then reverse transcribed into cDNA with the PrimeScriptTM RT Master Mix (RR036, Takara) according to the manufacturer's specifications. Copy numbers of the diatom-specific *rbcL* gene in extracted DNA and transcribed cDNA samples were quantified by quantitative PCR (qPCR) with standards of the diatom-specific *rbcL* gene, which were produced from the diatom *Thalassiosira weissflogii* (CCMP1336) in accordance with Endo et al. (2015).

2.11. Low temperature (77 K) emission spectra

The emission spectra at 77 K were measured on board using a custom-built portable emission spectrometer (Prášil et al., 2009) and measuring procedures described in Hill et al. (2012) with the following exceptions: the volume of seawater filtered on the 25 mm Whatman GF/F filters was 1.2 L. For each sample, six emission spectra were collected, using LEDs with different excitation wavelengths (390, 455, 470, 505, 530 and 590 nm). From each spectrum, a blank spectrum (measured using filter soaked in distilled water) was subtracted.

2.12. Statistical analyses

Statistical analyses were conducted using the SigmaPlot software program ver. 11.0 (SystStat Software, Inc.) except for the cluster analysis evaluating diatom community composition, which was carried out in the statistical software R (http://www.r-project.org). Spearman's correlation analysis was used to assess relationships between variables. Multiple linear regression analysis was conducted to determine the contributions of each diatom group to total Chl *a*. Cluster analysis was performed to investigate differences in community composition of diatoms using Bray-Curtis dissimilarity and an average clustering method. Statistically significant differences between clusters were assessed with a multivariate analysis of variance (MANOVA) test and the Wilks' lambda discriminant analysis.

3. Results

3.1. Hydrographic conditions

Sea surface temperatures (SST) observed during the KH15-1 expedition were generally low ranging from 0.0 to 1.6 °C whereas higher SST between 2.4 and 3.8 °C were observed during the AK15 cruise (Table 1). Values of sea surface salinity (SSS) were lower than 33 throughout both expeditions with the lowest SSS value of 32.1 being observed at Station AK15-1 (Table 1). Nutrients in surface waters were generally abundant during the KH15-1 expedition. The deepest mixed layer depth (MLD) of 28.6 m was found at Station Bio-10 whereas the shallowest MLD of 15.8 m was found at Station Bio-6 (Table 1). During the KH15-1 expedition, the depth (z) of the euphotic zone (Z_{eu}) was generally shallower than the MLD with Station Bio-6 being an exception (Table 1).

Stations on the shelf ($z \leq 100$ m) were classified as shelf COY, whereas those in rather oceanic regions ($z > 100$ m) were defined as offshore COY (Fig. 1 and Table 1). Warm water masses with a relatively high temperature of ~4 °C intruded into offshore COY waters from the western part of the coast between the isopycnal surfaces (σ_θ = 26.7–26.8; Appendix A). Thus, we refer to these stations as "Tokachi" to distinguish them from the other offshore and shelf sites.

3.2. Phytoplankton pigments

Concentrations of Chl *a* were generally < 1 mg m^{-3} except at bloom stations Station Bio-14, AK15-1 and AK15-2 (hereafter bloom stations) (Fig. 2a). Chl *a* concentrations were positively correlated with SST, but negatively with SSS (Table 2). Fuco, Peri, and diadinoxanthin (DD) were the predominant carotenoids (Appendix B) and were used in the following multiple regression to derive total Chl *a* according to:

$$[\text{Chl } a] = 2.00\ [\text{Fuco}] + 1.78\ [\text{Peri}] + 0.107, \quad (4)$$

wherein $n = 21$, $r^2 = 0.994$, t-value for Fuco = 56.0 ($p < 0.001$), t-value for Peri = 2.85 ($p < 0.05$), t-value for the constant = 2.12 ($p < 0.05$), and $F = 367$ ($p < 0.001$). Diatoms were predominant at all sampling stations contributing between 54 and 96% of total Chl *a* and > 90% at the bloom stations (Fig. 3a).

3.3. Size-fractioned chlorophyll a concentration

Nanophytoplankton dominated the phytoplankton community during the KH15-1 expedition with the exception of the bloom stations and Station Bio-7, where microphytoplankton (> 20 μm) dominated the phytoplankton assemblages. The lowest contribution (8.36% of total Chl *a*) of microphytoplankton was found at the farthest offshore Station Bio-10 (Fig. 3b).

3.4. Diatom community composition

The genera *Thalassiosira*, *Minidiscus*, *Skeletonema*, *Fragilariopsis,* and *Pseudo-nitzschia* dominated the diatom assemblages (Fig. 4) with minor contributions of diatoms belonging to the subdivision of Coscinodiscophytina. The genus *Thalassiosira* contributed > 40% to the total Chl *a* at the bloom stations (Bio-14, AK15-1 and AK15-2) and stations Bio-6 and Bio-7 (Fig. 4). Thus, the composition of the diatom community at these shelf COY stations was significantly different from that at other stations ($p < 0.01$, One-way MANOVA, Wilk's lambda; Fig. 5). At the offshore COY and Tokachi stations, diatom communities were characterized by the dominance of *Thalassiosira*, *Minidiscus* and/or *Fragilariopsis*.

3.5. Variable chlorophyll a fluorescence

$F_v/F_{m\ PAM}$ values determined with the PAM fluorometer varied between 0.17 and 0.55 (Fig. 2b), giving an average of 0.35 ± 0.11 across all sites. The highest and lowest $F_v/F_{m\ PAM}$ values were observed at Stations AK15-1 and Bio-10, respectively. Also, $F_v/F_{m\ PAM}$ was significantly correlated with Chl *a*, P^B_{max}, Φ_{Cmax}, and *PP*, ($p < 0.01$, < 0.01 < 0.05, and < 0.001, respectively; Spearman-Rank correlation, Table 3). During the KH15-1 expedition, F_v/F_m measured by FRR fluorometry ($F_v/F_{m\ FRRf}$) (Appendix C) showed a similar spatiotemporal variation as $F_v/F_{m\ PAM}$ ($\rho = 0.483$, $n = 20$, $p < 0.05$, Spearman-Rank correlation), although a large difference between $F_v/F_{m\ FRRf}$ and F_v/F_m

Table 1
Sampling conditions and hydrographic and optical data during the KH15-1 and AK15 expeditions.

Sampling date	Station	Water mass	Bottom depth (m)	SST (°C)	SSS	NO_3 (μM)	NO_2 (μM)	NH_4 (μM)	PO_4 (μM)	SiO_2 (μM)	K_d(PAR) (m^{-1})	Z_{eu} (m)	MLD (m)
2015.03.08	Bio-1	Offshore	852	0.03	32.58	21.29	0.18	0.69	1.81	35.50	0.105	44.1	26.6
2015.03.09	Bio-2	Offshore	564	0.39	32.71	22.20	0.11	0.44	1.93	35.38	0.12	38.5	29.9
2015.03.13	Bio-4	Tokachi	103	0.42	32.36	18.43	0.23	0.71	1.71	33.73	0.291	15.8	27.3
2015.03.14	Bio-6	Shelf	100	0.93	32.17	19.77	0.18	1.43	1.54	39.24	0.363	12.7	15.8
2015.03.15	Bio-7	Shelf	97	0.67	32.55	20.64	0.18	1.02	1.85	36.25	0.145	31.7	20.2
2015.03.17	Bio-9	Offshore	1477	0.64	32.38	18.13	0.23	0.54	1.76	32.19	0.159	28.9	19.5
2015.03.18	Bio-10	Offshore	4100	1.60	32.78	24.70	0.17	UD	2.21	43.22	0.087	52.6	28.6
2015.03.19	Bio-11	Shelf	100	0.85	32.71	23.60	0.16	0.27	2.10	41.01	0.119	38.9	20.1
2015.03.20	Bio-12	Offshore	529	0.63	32.62	27.21	0.21	0.35	2.45	48.93	0.137	33.9	23.6
2015.03.21	Bio-13	Tokachi	1084	1.47	32.62	24.53	0.27	0.29	2.30	46.03	0.131	35.0	18.9
2015.03.22	Bio-14	Shelf	100	0.56	32.52	31.43	0.33	0.27	2.94	59.28	0.143	32.1	19.5
2015.04.16	AK15-1	Shelf	33	3.84	32.06	0.83	0.05	UD	0.34	4.12	ND	ND	27.8
2015.04.17	AK15-2	Shelf	32	2.41	32.22	2.01	0.08	UD	0.48	1.78	ND	ND	21.4

SST: Sea surface temperature; SSS: Sea surface salinity; NO_3, NO_2, NH_4, PO_4, and SiO_2: Concentration of nitrate, nitrite, ammonium, phosphate, and silicate; K_d(PAR): Vertical attenuation coefficient of downward photosynthetically available radiation (PAR); Z_{eu}: Euphotic layer depth; MLD: Mixed layer depth.

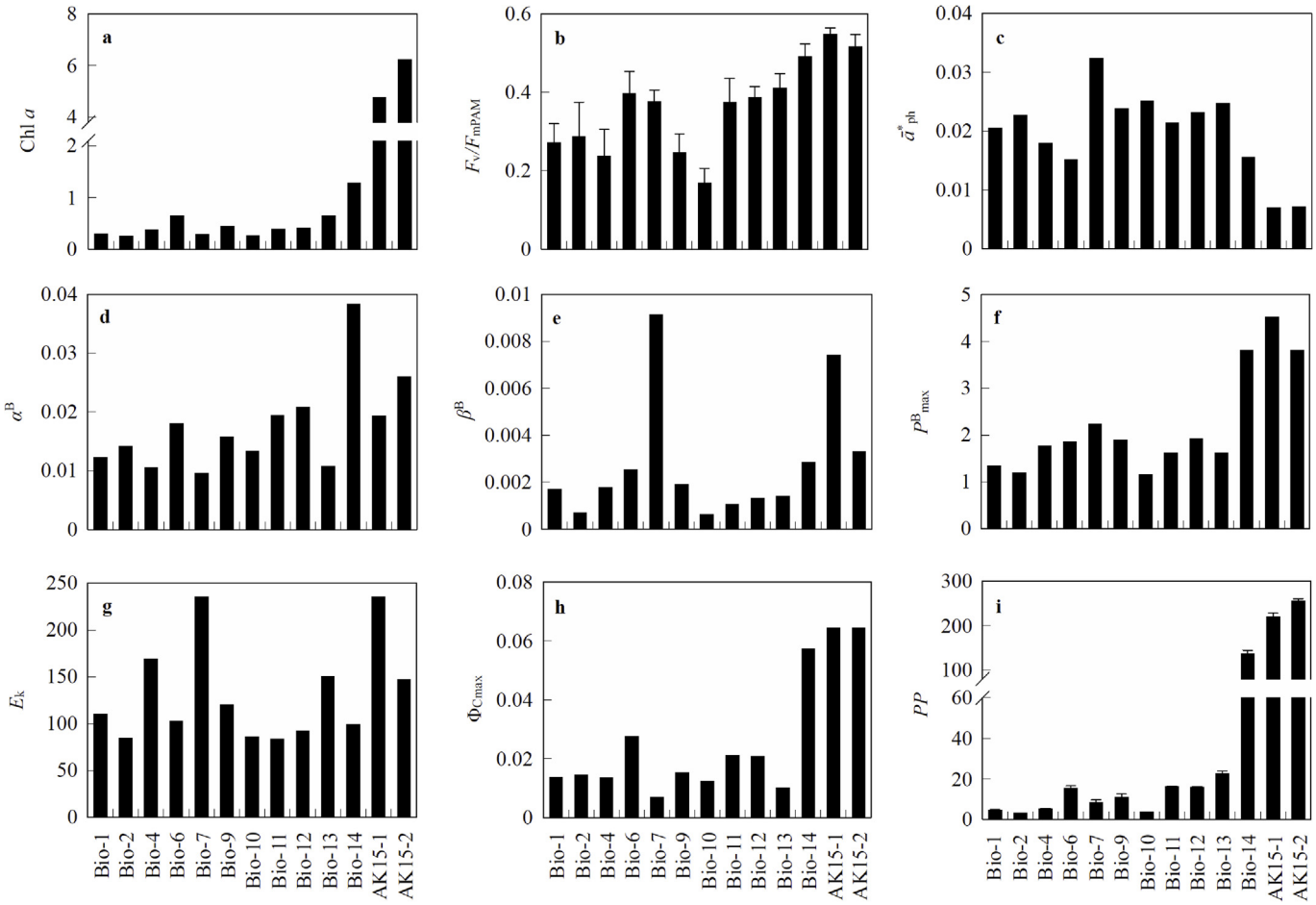

Fig. 2. Photosynthetic parameters obtained from *P-E* curve experiments at *in situ* sampling stations. Chl *a*: Chl *a* concentration [mg m^{-3}]; F_v/F_{mPAM}: Maximum quantum yield of PSII obtained by PAM fluorometry; $\bar{a}^*$ph: Chl *a*-normalized light absorption coefficient of phytoplankton [m^2 mg Chl *a*]; α^B: Initial slope of *P-E* curve [mg C mg Chl a^{-1} h^{-1} (μmol photons m^{-2} s^{-1}) $^{-1}$]; β^B: Photoinhibition index [mg C mg Chl α^{-1} h^{-1} (μmol photons m^{-2} s^{-1}) $^{-1}$]; P^B_{max}: Maximum photosynthetic rate [mgC mgChl α^{-1} h^{-1}]; E_k: Light saturation index [μmol photons m^{-2} s^{-1}]; Φ_{Cmax}: Maximum quantum yield for carbon fixation [mol C mol photons^{-1}]; *PP*: Primary productivity [mg C m^{-3} day^{-1}]. Error bars are standard deviations, $n \geq 3$.

$_{PAM}$ was observed at Station Bio-1. Values of the functional absorption cross-section for PSII (σ_{PSII}) varied between 2.43 and 3.78 nm^2 $PSII^{-1}$. The lowest and highest values were observed at Stations Bio-14 and Bio-2, respectively, which deviated from values at the other stations. A much larger variability, however, was observed in the concentration of functional PS II centers [RCII], which varied between 0.49×10^{-9} and 5.57×10^{-9} mol m^{-3} at Station Bio-1 and Bio-14, respectively (Appendix C). The latter was also the site with the highest Chl *a* concentration.

Table 2
Spearman-rank correlation coefficients between photosynthetic, environmental and community composition data.

	Chl *a*	F_v/F_{mPAM}	α^B	β^B	P^B_{MAX}	E_k	$\bar{a}^*_{ph}$	Φ_{Cmax}	PP
SST	**0.57***	0.52	0.22	0.27	0.35	0.26	−0.14	0.28	**0.57***
SSS	**−0.66***	−0.50	−0.20	**−0.83*****	**−0.76****	**−0.65***	**0.70****	−0.55	−0.50
NO_3	−0.29	−0.13	0.12	**−0.57***	−0.48	**−0.60***	0.45	−0.20	−0.17
NO_2	0.08	−0.10	−0.14	−0.03	−0.08	0.07	0.28	−0.32	−0.04
NH_4	−0.36	−0.33	−0.51	0.15	−0.15	0.20	0.19	−0.41	−0.45
PO_4	−0.26	−0.13	0.08	−0.52	−0.33	−0.51	**0.56***	−0.34	−0.12
SiO_2	−0.12	0.00	0.11	−0.30	−0.25	−0.43	0.39	−0.23	−0.03
MLD	−0.49	−0.32	−0.15	−0.31	−0.24	−0.12	−0.02	−0.09	−0.44
rbcL	0.41	0.29	0.19	0.15	0.33	0.27	0.00	0.20	0.47
%Micro	**0.57***	**0.61***	0.46	**0.77****	**0.91*****	0.44	**−0.59***	**0.59***	**0.66***
%Nano	−0.31	−0.63*	−0.33	−0.44	−0.53	−0.23	0.28	−0.35	−0.47
%Pico	**−0.69***	**−0.49**	**−0.58***	**−0.60***	**−0.77****	−0.27	**0.80****	**−0.80****	**−0.61***
%Diatom	**0.61***	0.40	0.53	0.34	0.54	0.17	**−0.57***	**0.61***	0.64*
%Dino	−0.35	−0.22	−0.52	−0.19	−0.35	0.04	0.52	−0.59*	−0.30
%*Thalassiosira*	**0.70***	**0.76****	0.34	**0.84*****	**0.74****	0.48	−0.51	0.47	**0.65***
%*Minidiscus*	−0.80	**−0.75****	−0.37	**−0.67***	**−0.59***	−0.39	0.52	−0.51	**−0.66***
%*Skeletonema*	−0.21	−0.29	−0.45	−0.17	−0.25	0.17	0.60*	**−0.64***	−0.27
%*Fragilariopsis*	−0.45	**−0.65***	−0.45	**−0.73****	**−0.77****	−0.32	**0.65***	**−0.61***	−0.49
%*Pseudo-Nitzschia*	−0.45	−0.41	−0.18	**−0.83*****	**−0.72****	−0.50	0.25	−0.29	−0.47
%Coscinodiscophytina	0.52	0.53	0.53	0.42	**0.69****	0.21	**−0.59***	**0.58***	**0.62***

Bold values indicate significant relationships with asterisks denoting different significance levels: * = 0.05, ** = 0.01, *** = 0.001, n = 13.
SST: Sea surface temperature; SSS: Sea surface salinity; NO_3, NO_2, NH_4, PO_4, and SiO_2: Concentration of nitrate, nitrite, ammonium, phosphate, and silicate; MLD: Mixed layer depth; *rbcL*: Diatom-specific *rbcL* gene expression, Micro: microphytoplankton, Nano: nanophytoplankton, Pico: Picophytoplankton, Dino: dinoflagellates, Other: other functional groups than diatoms and dinoflagellates. The % denotes relative contribution of given phytoplankton groups.

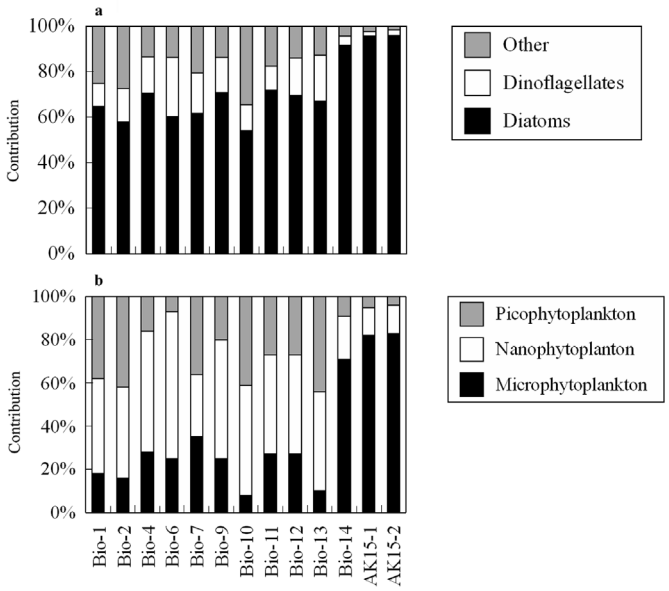

Fig. 3. Relative contribution of phytoplankton groups to Chl *a* (a) at the class level class at the different sampling stations determined by multiple regression analysis based on diagnostic pigment signatures and (b) at the level of size class of phytoplankton determined by size-fractioned Chl *a* measurement.

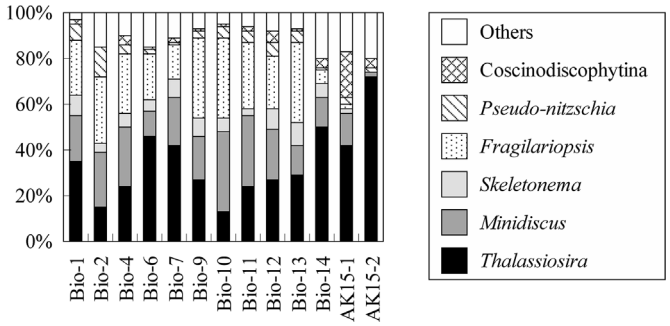

Fig. 4. Relative contribution of diatom community composition to total number of sequences determined by the next-generation sequencing method at *in situ* sampling stations.

3.6. Light absorption coefficient of phytoplankton

The Chl *a*-normalized light absorption coefficient for phytoplankton ($\bar{a}^*_{ph}$) at the bloom stations as well as at Station Bio-6 were relatively low compared to the other sites of this study (Fig. 2c). In particular, values of $\bar{a}^*_{ph}$ obtained during the AK15 cruise were one order of magnitude smaller than those during the KH15-1 expedition.

3.7. Low temperature (77 K) emission spectra

We have observed significant variability among the 77 K emission spectra collected at each station. The variability can be linked to species composition and the physiological state of phytoplankton. An example of emission spectra in the 660–700 nm region is given in Appendix D, panels A and B. The phytoplankton emission in this spectral region is composed of several overlapping bands: the major band peaks at 685 nm and originates from PSII reaction centers, the band at 695 nm originates from active PSII containing CP47 (Suggett et al., 2009; D'Haene et al., 2015) and in some cases less intense bands at 675 and 680 nm were observed. In eukaryotic phytoplankton, the 680 nm band originates from loosely coupled antenna pigments with less efficient energy transfer to the PSII reaction center. The 675 nm band (Appendix D, panel B) is specific for emission from Peri containing peripheral peridinin-chlorophyll *a*-protein (PCP) antenna proteins in dinoflagellates and is excited only by the 500–600 nm wavelengths absorbed by PCP (Hill et al., 2012). Using simple analysis of the emission spectra based on the measured emission intensities at given wavelength, we have observed correlation (r^2 = 0.598) between the relative content of Peri (determined by UHPLC) and the increase of emission at 675 nm (Appendix D, panel C) or between the functional cross-section of PSII measured by FRR fluorometry and the intensity of the emission in the 675–680 nm region (r^2 = 0.732, see Appendix D, panel D). The increased emission band around 695 nm, indicating phytoplankton with active PSII (Suggett et al., 2009), was observed only at station Bio-14 (Appendix D, panel B).

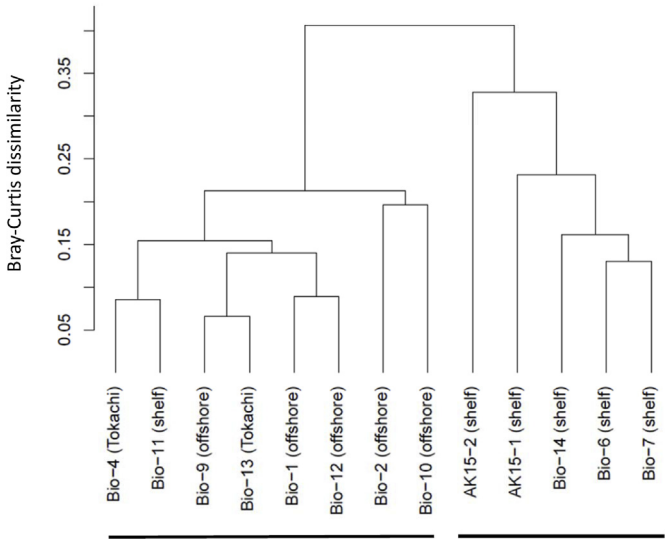

Fig. 5. Dendrogram of the cluster analysis of diatom community composition determined with the next-generation sequencing method. Clustering is based on Bray-Curtis dissimilarity and the group average method. The cluster on the right-hand side includes samples from shelf COY water, which had a community composition significantly different from the other sites (One-way MANOVA, Wilk's lambda, $p < 0.01$).

3.8. P-E curves and their photosynthetic parameters

Values of α^B varied between 0.00949 and 0.0383 (mg C mg Chl a^{-1} h^{-1}) (μmol photons m^{-2} s^{-1})$^{-1}$ (Fig. 2d), and the β^B values ranged between 0.000628 and 0.00912 (mg C mg Chl a^{-1} h^{-1}) (μmol photons m^{-2} s^{-1})$^{-1}$ (Fig. 2e). P^B_{max} values, however, were relatively constant and ranged between 1 and 2 mg C mg Chl a^{-1} h^{-1} except at the bloom stations (Fig. 2f). The E_k values varied from 83.2 to 235.0 μmol photons m^{-2} s^{-1} giving an average value with standard deviation of 131.8 ± 53.2 μmol photons m^{-2} s^{-1} (Fig. 2g). Values of Φ_{Cmax} were rather constant (0.0068–0.0275) except at the bloom stations (Fig. 2h). The P^B_{max} and E_k showed negative correlations with respect to SSS (Table 2).

3.9. Primary productivity

Primary productivity (*PP*) at all sampling stations ranged between 3.56 and 255.40 mg C m^{-3} d^{-1} (Fig. 2i) being highest at the bloom stations. Lowest *PP* was observed at Station Bio-1, which also had the lowest SST values (Fig. 2i, Table 1). Also note that *PP* was significantly correlated with SST and Chl *a* ($p < 0.05$ and < 0.001, respectively, Spearman-Rank correlation, Tables 2 and 3).

3.10. On-deck temperature-controlled bottle incubation experiments

Phytoplankton pigment signatures revealed that algal community composition calculated from Eq. (4) changed relatively little (<5%) during our incubations, except at Station Bio-6 where the contribution of dinoflagellates increased from 39.7% to 47.7% in the 7 °C treatment (Fig. 6). Similarly, little changes in the composition of diatoms occurred throughout all experiments except at Station Bio-13 (Tokachi waters) where growth of *Minidiscus* was stimulated in the 7 °C treatment (Fig. 7).

At the end of the incubation, the *P-E* curve parameters varied differently between incubations at different stations (Fig. 8). Values of α^B increased by ca. three-fold in the 7 °C treatment during the Bio-7 experiment, while changes at the other sites were much less pronounced (Fig. 8a). The P^B_{max} values increased in both treatments at most sites. The exception was Station Bio-10, where P^B_{max} showed a slight decrease

Table 3
Spearman-rank correlation coefficients between *P-E* curve parameters.

	Chl *a*	$\bar{a}^*_{ph}$	F_v/F_{mPAM}	α^B	β^B	P^B_{max}	E_k	Φ_{Cmax}
F_v/F_{mPAM}	**0.80****	–	–					
$\bar{a}^*_{ph}$	**−0.62***	−0.53						
α^B	0.60*	0.54	−0.55	–				
β^B	**0.56***	**0.58***	−0.40	0.09	–			
P^B_{max}	**0.72****	**0.72****	−0.48	0.50	**0.84*****	–		
E_k	0.33	0.28	−0.09	−0.42	**0.75****	0.51	–	
Φ_{Cmax}	**0.69***	**0.62****	**−0.83*****	**0.87*****	0.34	**0.61***	−0.15	–
PP	**0.92*****	**0.88*****	−0.53	**0.64***	0.52	**0.75****	0.25	**0.68****

Bold numbers indicate significant relationship between given parameters. Significance levels are denoted by numbers of asterisks: * = 0.05, ** = 0.01, *** = 0.001, $n = 13$.
α^B: Initial slope of *P-E* curve [mg C mg Chl a^{-1} h^{-1} (μmol photons m^{-2} s^{-1})$^{-1}$]; β^B: Photoinhibition index [mg C mg Chl a^{-1} h^{-1} (μmol photons m^{-2} s^{-1})$^{-1}$]; P^B_{max}: Maximum photosynthetic rate [mgC mgChl a^{-1} h^{-1}]; E_k: Light saturation index [μmol photons m^{-2} s^{-1}]; Chl *a*: Chl *a* concentration [mg m^{-3}]; $\bar{a}^*_{ph}$: Chl *a*-normalized light absorption coefficient of phytoplankton [m^2 mg Chl *a*]; Φ_{Cmax}: Maximum quantum yield for carbon fixation [mol C mol photons^{-1}]; *PP*: Primary productivity [mg C m^{-3} day^{-1}].

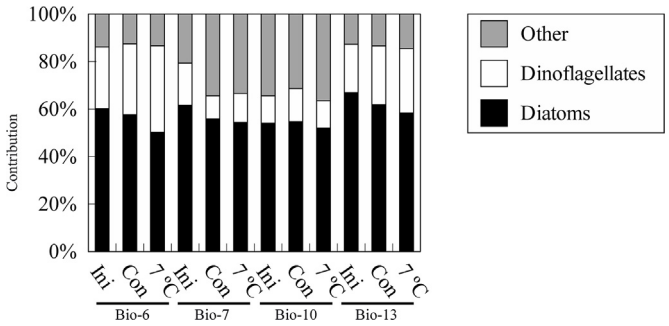

Fig. 6. Relative contribution of phytoplankton groups to Chl *a* at the class level during the temperature-controlled incubation experiments determined by the multiple regression analysis based on diagnostic pigments.

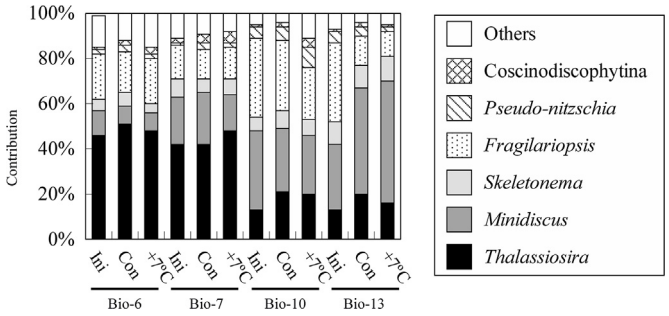

Fig. 7. Relative contribution of diatom community composition to total number of sequences during the temperature-controlled incubation experiments determined with the nextgeneration sequencing method.

in both the control and 7 °C treatment (Fig. 8c). Changes in E_k were variable increasing after incubation at 7 °C during experiments at stations Bio-6 and Bio10, but decreasing at Station Bio-7 (Fig. 8d). Φ_{Cmax} was highest in the +7 °C treatment at Stations Bio-7 and Bio-13 (Fig. 8f). At the shelf COY (Bio-6 and Bio-7) and Tokachi (Bio-13) stations where the water was <100 m deep, values of the diatom-specific *rbcL* gene expression for the +7 °C treatments were higher than those of the controls (Fig. 8g). Values of $\bar{a}^*_{ph}$ and F_v/F_{mPAM} varied little among treatments at all stations (Fig. 8e, h).

4. Discussion

4.1. Hydrography

Cold, low-salinity waters extended completely across our sampling sites throughout the observation period i.e., early spring (Table 1). Following the water mass definitions in this study area proposed by Ohtani (1971), OY waters were not detected. The results were similar to observations of Kasai et al. (1997) who demonstrated that COY waters extended from the coast off Hokkaido to the offshore station at 42° 40′ N, 144° 55′ E in March 1990, 1991, and 1992.

4.2. Abundance and community composition of spring phytoplankton in the COY

The temporal variation in Chl *a* concentration suggests that the sampling period covered both, the pre-bloom and bloom phase (Fig. 2a), with the former being characterized by low Chl *a* concentrations (<1 mg m^{-3}). The subsequent increase in Chl *a* concentration during the AK15 expedition represented the spring bloom at the shelf COY stations (Fig. 2a), which matches the observations of Kasai et al. (1997) who also reported peaks in Chl *a* in COY waters in April. Kasai et al. (1997) also proposed that shoaling of the MLD due to water-column stratification may be an important factor for bloom initiation. In this study, however, there was no significant relationship between any of the photosynthetic parameters (including Chl *a*) and MLD (Table 2).

The substantial increases in Chl *a* and Fuco at the bloom stations indicated that the blooms on the COY shelf were dominated by diatoms (Fig. 3a and Appendix B). The large increase in the relative contribution of microphytoplankton to the total phytoplankton also supports this notion (Fig. 3b). Interestingly, our DNA sequencing analysis showed that the composition of the diatom assemblages in most of the shelf COY stations differed from those of other water masses (Figs. 4 and 5). Because the shelf COY stations were located in relatively shallow waters, resuspension of benthic diatoms from shelf sediments might affect either or both community composition and bloom formation (e.g. McQuoid and Godhe, 2004), although no information on the composition of the benthic algal community is available for our study area. The discrimination between the shelf COY and other waters masses was based mainly on the presence and dominance of *Thalassiosira* (Fig. 4). Shinada et al. (1999) observed *Thalassiosira* blooms in Funka Bay when COY waters intruded into the bay in early spring. In this study, the genus *Thalassiosira* was the bloom-forming species in the shelf COY waters indicated by the contribution of *Thalassiosira* becoming high at the bloom stations (Fig. 4). The genera *Fragilariopsis* and *Minidiscus* were relatively abundant in offshore COY and Tokachi waters (Fig. 4). Suzuki et al. (2011) reported that the genus *Fragilariopsis* was abundant in OY waters. The substantial abundance of *Minidiscus*, however, has not been reported in both COY and OY waters likely because the genus *Minidiscus* can be overlooked with conventional light microscopy due to its small size, i.e., nanophytoplankton (Hasle and Syvertsen, 1996). Although blooms of the genus *Chaetoceros* are commonly and annually observed during the bloom period (Mochizuki et al., 2002; Hattori-Saito et al., 2010; Suzuki et al., 2011), the contributions of *Chaetoceros* to the diatom assemblages (as determined with the next-generation sequencing method) were generally low and negligible (<4%) (Fig. 4). Hattori-Saito et al. (2010) also observed the predominance of *Thalassiosira* at the pre-bloom station at COY and OY regions, whereas *Cheatoceros* outcompeted other taxa at the OY bloom station. Both pigment analysis (presence of peridinin, Appendix B) and 77 K emission spectroscopy (Appendix D, panel C) indicated increased presence of dinoflagellates at near-coast stations Bio-6, 7 and 4.

4.3. Photosynthetic physiology of spring phytoplankton in the COY

At the bloom stations with high Chl *a* concentrations, we also observed high P^B_{max}, Φ_{Cmax}, and *PP* values (Fig. 2a, f, h, and i), suggesting that the photophysiological states of phytoplankton had improved from the pre-bloom period. In addition, P^B_{max} showed a significant correlation with other photosynthetic parameters, i.e. F_v/F_{mPAM}, Φ_{Cmax}, and *PP* (Table 3). In turn, it should be noted that the F_v/F_{mPAM} values correlated with *PP* and Chl *a* concentration as well (Table 3). Consequently, light reaction processes in PSII are important for the underlying mechanisms such as coupling of antenna pigments to PSII reaction centers (discussed below) to control *PP* and phytoplankton biomass during the observation period. Indeed, the increase in [RCII] (i.e., the concentration of PSII reaction centers) at Station Bio-14 indicated the significance of light reaction processes in the bloom development (Appendix C). We also observed, for the first time, correlations between the effective absorption cross-section of PSII (σ_{PSII}) and the relative intensity of the emission band at 680 nm that forms a low-wavelength shoulder of the main emission band assigned to PSII (see Appendix D, panels A and D). We assign this band to emission from antenna chlorophylls that are not tightly coupled to PSII reaction centers. We note that phytoplankton with high σ_{PSII} also shows a higher proportion of loosely coupled antenna pigments. Interestingly, at the high-chlorophyll station Bio-14 we detected both, low values of σ_{PSII}, a low proportion of uncoupled antenna and a significant increase in active PSII (see emission at 695 nm, Appendix D, panels A and B). This enhanced coupling of antenna pigments at Station Bio-14 could lead the high F_v/F_m, P^B_{max} and *PP* values

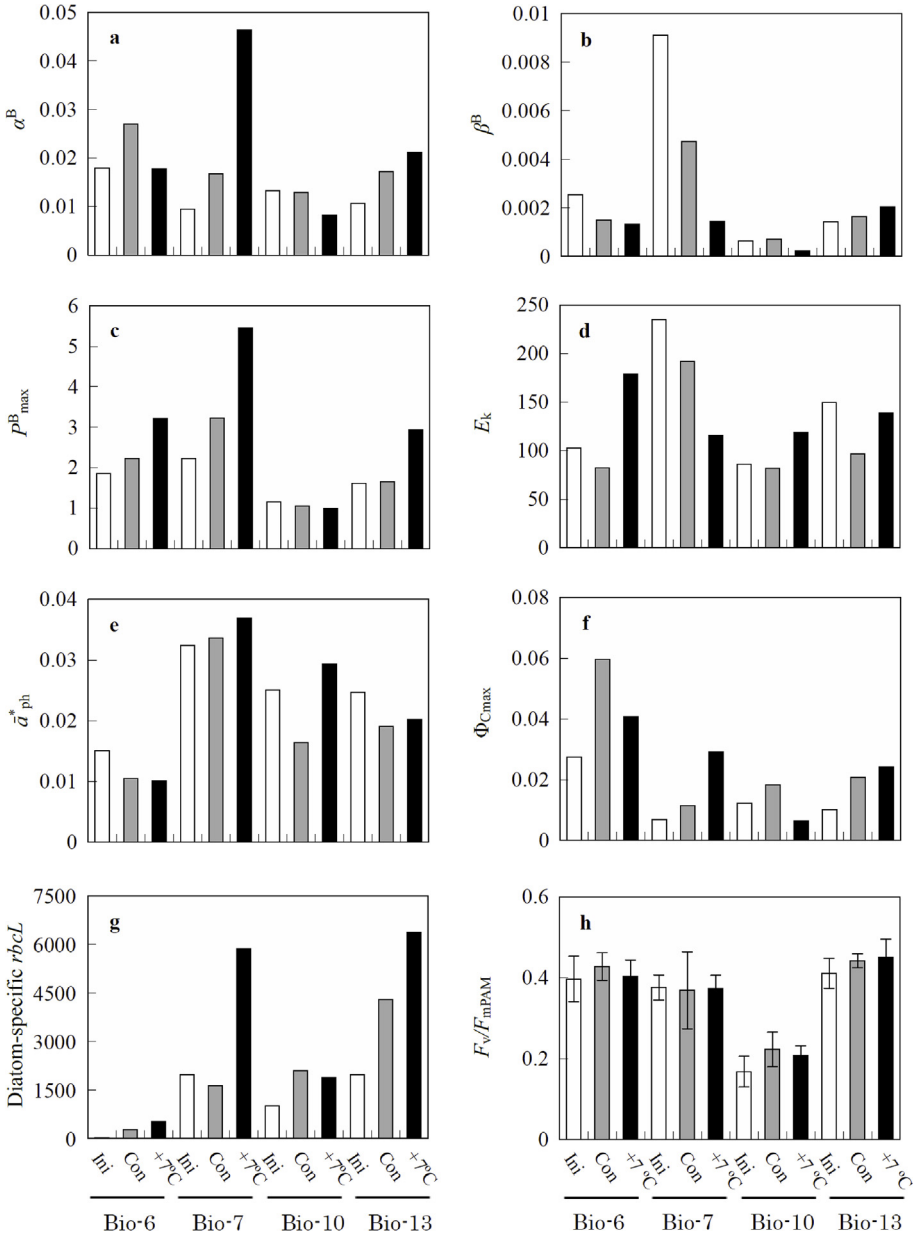

Fig. 8. Photosynthetic parameters during the temperature-controlled incubation experiments. The open bars indicate values of initial bottles, shaded bars indicate values of control treatments, and closed bars show values of the +7 °C treatment. (a) α^B: Initial slope of *P-E* curve [mg C mg Chl a^{-1} h^{-1} (μmol photons m^{-2} s^{-1}) $^{-1}$]; (b) β^B: Photoinhibition index [mg C mg Chl a^{-1} h^{-1} (μmol photons m^{-2} s^{-1}) $^{-1}$]; (c) P^B_{max}: Maximum photosynthetic rate [mgC mgChl a^{-1} h^{-1}]; (d) E_k: Light saturation index [μmol photons m^{-2} s^{-1}]; (e) $\bar{a}^*_{ph}$: Chl *a*-normalized light absorption coefficient of phytoplankton [m^2 mg Chl *a*]; (f) Φ_{Cmax}: Maximum quantum yield for carbon fixation [mol C mol photons^{-1}]; (g) Diatom-specific *rbcL*: Transcription level of the diatom-specific *rbcL* gene (cDNA copies/DNA copies); (h) F_v/F_{mPAM}: Maximum quantum yield of PSII obtained by PAM fluorometry. Error bars are standard deviations, n ≥ 3.

(Fig. 2b, f, and i), which might be associated with bloom development in COY waters. Interestingly, the SSS showed significant negative correlations with the photosynthetic parameters including P^B_{max} values and Chl *a* concentration (Table 2), which implies the surface phytoplankton assemblages in low saline shelf COY waters had relatively higher carbon fixation rates. Co-variations of the P^B_{max} and α^B values were not found in this study (Table 3), indicating E_k-dependent variability (Behrenfeld et al., 2004) in photosynthesis. According to Behrenfeld et al. (2004), the physiological mechanisms responsible for E_k-dependent variability generally involve acclimation strategies aimed at maximizing growth under variable light conditions. On the other hand, in the OY region, E_k-independent variability, which is the result of co-variation in P^B_{max} and α^B, was observed from March to May by Isada et al. (2009) and in the post-bloom phase by Yoshie et al. (2010). Additionally, Yoshie et al. (2010) pointed out that water temperature and ammonium levels significantly affected the E_k-independent variability. In this study, water temperatures of COY remained relatively low (< 4 °C; Table 1) and ammonia did not influence any photosynthetic parameters (Table 2). The SST values, however, showed significant positive correlations with Chl *a* and *PP*, suggesting that temperature was a significant driver for biomass and primary production. The contribution of microphytoplankton to total Chl *a* correlated positively with the photosynthetic parameters including Chl *a*, F_v/F_{mPAM}, P^B_{max}, and *PP* (Table 2), indicating that microphytoplankton contributed considerably to bloom formation in this area. The contributions of diatoms to Chl *a* concentrations, however, did not show any significant correlation with these photosynthetic parameters (Table 2). The results imply that some specific diatoms had different photosynthetic strategies

and formed the bloom in April. In fact, the contributions of *Thalassiosira* to the total diatoms showed a positive relationship with P^B_{max} among the diatom groups (Table 2), which suggests the genus *Thalassiosira* bloomed in COY waters.

4.4. Physiological response of phytoplankton to temperature in COY waters

In the temperature-controlled experiments, the phytoplankton assemblages showed different responses among stations. Changes in the P^B_{max} values with the increase in temperature were prominent for the phytoplankton assemblages in the shelf COY (Stations Bio-6 and -7) and the Tokachi (Station Bio-13) waters, whereas no increase in P^B_{max} was observed for those in the offshore COY at Station Bio-10 (Fig. 8c). Similarly, the diatom-specific *rbcL* cDNA copies normalized by their DNA copies for the shelf COY and Tokachi assemblages also notably increased after the temperature change (Fig. 8g), suggesting that the transcriptional levels of the diatom-specific *rbcL* gene could be upregulated by the increase in temperature at these stations. Interestingly, the offshore COY assemblages showed little change in the transcription level of diatom-specific *rbcL* as well as P^Bmax (Fig. 8c, g). These concomitant increases indicate that the enhancement of the P^B_{max} for the shelf COY and Tokachi assemblages could be caused by the increases in the transcription level of the large subunit of RuBisCO with temperature. This hypothesis is supported by the fact that P^B_{max} values are controlled by the activity of RuBisCO (Li et al., 1984; Descolas-Gros and de Billy, 1987; Raven and Geider, 1988). In general, the optimal temperature of RuBisCO (40–50 °C) (Descolas-Gros and de Billy, 1987; Young et al., 2015) was far above the *in situ* SST (0–4 °C) observed in this study, and, thus, its activity would increase exponentially with temperature up to a certain point (Descolas-Gros and de Billy, 1987; Crafts-Brandner and Salvucci, 2000). The temperature increase, therefore, enhanced both the expression of the *rbcL* gene and the catalytic efficiency of RuBisCO, which eventually led to high carbon fixation rates. The genus *Thalassiosira* became the bloom-forming group in the shelf COY (Fig. 4), so the genus *Thalassiosira* might be capable of responding rapidly to environmental changes such as an increase in temperature. Their rapid growth, however, was not observed in the short-term incubation experiments. On the other hand, relative contributions of the genus *Minidiscus* to the diatom assemblages increased at the Tokachi station (Bio-13) after the temperature increase (Fig. 7). Because the physiological and phylogenic information on *Minidiscus* were limited, further studies on this group are needed to understand their rapid increase.

Among the other photosynthetic parameters from *P-E* curve analyses, α^B was considered to have little variation with temperature because α^B is an index for the capability of carbon fixation in light-limited environments and, thus, reflects mainly the light-dependent reactions of photosynthesis (Platt and Jassby, 1976; Kiefer and Reynolds, 1992; Kolber and Falkowski, 1993). In the incubation experiments at Stations Bio-7 and Bio-13, however, increases in α^B values were observed with temperature (Fig. 8a). Although similar results were also observed in the previous studies (e.g. Verity, 1981; Palmisano et al., 1987), the mechanisms are still unclear. As estimated from the small variations in F_v/F_{mPAM} (Fig. 8h), temperature negligibly affected the maximum quantum yield of PSII for the phytoplankton assemblages at all stations in this study, but the light-harvesting property of PSII could be affected by temperature. Because α^B values relate to σ_{PSII} and the number of photosynthetic antennae (n) with varying non-photochemical quenching (e.g., Sakshaug et al., 1997), temperature might affect the light harvesting property of PSII i.e., n and σ_{PSII} (e.g., Mock and Hoch, 2005; Ralph et al., 2005).

Acknowledgments

The authors are grateful to Dr. J. Nishioka for ship board assistance, nutrient analysis, and his valuable comments. Dr. T. Hirawake is thanked for sharing his data on surface PAR and primary productivity. We wish to acknowledge Mr. Weichen Qiu for his assistance in the 77 K fluorescence measurements. Thanks are also extended to the officers and crew of R/V *Hakuho Maru* and TR/V *Misago Maru*. This study was partly supported by the JSPS Grants-in-Aid for Scientific Research (A) (JP17H00775) and (B) (JP18H03352). O.P. and E.L. were partly supported by projects Algatech (CZ.1.05/2.1.00/03.0110) and Algatech Plus (MSMT LO 1416).

Appendices

Appendix A
Potential temperature (θ) between the isopycnal surfaces σ_θ = 26.7 and 26.8 at all sampling stations.

Station	θ between σ_θ = 26.7–26.8
Bio-1	0.6
Bio-2	0.6
Bio-4	3.5
Bio-6	2.3
Bio-7	1.1
Bio-9	1.3
Bio-10	1.0
Bio-11	0.9
Bio-12	1.3
Bio-13	4.0
Bio-14	0.5
AK15-1	ND
AK15-2	ND

Appendix B

Pigment composition determined with the UHPLC analysis method (Suzuki et al., 2015) at all stations.

Station	Chl c_3	Chl c_2	Chlide *a*	Peri	19′-BF	Fuco	Neo	Prasino	Viola	19′-HF	DD	Allo	DT	Zea	Lut	Chl *b*	Chl *a*	α, β-caro
Bio-1	0.0324	0.0467	0.0240	0.0248	0.0286	0.138	0.0060	0.0114	0.0104	0.0210	0.0536	0.0015	0.0037	0.0041	0.0016	0.0393	0.286	0.0144
Bio-2	0.0321	0.0522	0.0213	0.0327	0.0337	0.113	0.0061	0.0094	0.0104	0.0314	0.0473	UD	0.0034	0.0042	0.0010	0.0365	0.248	0.0169
Bio-4	0.0336	0.0907	0.0411	0.0725	0.0208	0.281	0.0103	0.0155	0.0131	0.0163	0.0755	UD	0.0059	0.0090	0.0026	0.0600	0.371	0.0310
Bio-6	0.0231	0.0900	0.0428	0.113	0.0156	0.232	0.0086	0.0112	0.0124	0.0093	0.0820	UD	0.0104	0.0091	0.0016	0.0470	0.639	0.0321
Bio-7	0.0199	0.0555	0.0185	0.0522	0.0132	0.160	0.0056	0.0098	0.0089	0.0086	0.0593	UD	0.0094	0.0047	0.0016	0.0459	0.280	0.0240
Bio-9	0.0323	0.0951	0.0500	0.0687	0.0238	0.277	0.0099	0.0175	0.0186	0.0167	0.0822	0.0018	0.0071	0.0076	0.0032	0.0667	0.438	0.0285
Bio-10	0.0257	0.0354	0.0251	0.0202	0.0254	0.0839	0.0038	0.0087	0.0038	0.0300	0.0379	UD	0.0116	0.0072	0.0023	0.0306	0.256	0.0112
Bio-11	0.0360	0.0828	0.0380	0.0371	0.0344	0.219	0.0077	0.0128	0.0157	0.0386	0.0624	0.0006	0.0052	0.0061	0.0031	0.0559	0.386	0.0273
Bio-12	0.0408	0.0985	0.0499	0.0706	0.0388	0.265	0.0095	0.0182	0.0216	0.0288	0.0902	0.0016	0.0089	0.0087	0.0032	0.0753	0.404	0.0314
Bio-13	0.0743	0.1506	0.0686	0.0964	0.0841	0.282	0.0104	0.0169	0.0238	0.0784	0.127	UD	0.0098	0.0077	0.0058	0.0761	0.647	0.0421
Bio-14	0.0537	0.2949	0.1635	0.0556	0.0389	1.13	0.0148	0.0202	0.0210	0.0249	0.162	0.0018	0.0153	0.0097	0.0043	0.100	1.28	0.0679
AK15-1	0.0233	0.0064	UD	0.0469	UD	2.11	0.0060	UD	UD	0.0106	0.219	0.110	0.0108	0.0083	UD	0.0631	4.76	0.0794
AK15-2	0.0195	0.0068	UD	0.0880	UD	3.08	0.0101	UD	UD	UD	0.218	0.0661	0.0222	UD	UD	0.0634	6.22	0.0920
Bio-6_Ini	0.0231	0.0900	0.0428	0.113	0.0156	0.232	0.0086	0.0112	0.0124	0.0093	0.0820	UD	0.0104	0.0091	0.0016	0.0470	0.639	0.0321
Bio-6_Con	0.0113	0.0113	UD	0.143	0.0139	0.245	UD	0.0124	UD	0.0132	0.0627	0.0506	UD	UD	UD	0.0361	0.801	0.0194
Bio-6_+7 °C	UD	UD	UD	0.164	0.0130	0.201	0.0042	0.0111	UD	0.0123	0.0534	0.0481	UD	UD	UD	0.0308	0.740	0.0180
Bio-7_Ini	0.0199	0.0555	0.0185	0.0522	0.0132	0.160	0.0056	0.0098	0.0089	0.0086	0.0593	UD	0.0094	0.0047	0.0016	0.0459	0.280	0.0240
Bio-7_Con	0.0103	0.0146	UD	0.0170	0.0053	0.0867	0.0024	0.0047	UD	0.0047	0.0138	0.0101	UD	UD	UD	0.0136	0.222	0.0054
Bio-7_+7 °C	UD	UD	UD	0.0219	0.0056	0.0870	0.0029	0.0050	UD	0.0049	0.0133	0.0094	UD	UD	UD	0.0152	0.229	0.0053
Bio-10_Ini	0.0257	0.0354	0.0251	0.0202	0.0254	0.0839	0.0038	0.0087	0.0038	0.0300	0.0379	UD	0.0116	0.0072	0.0023	0.0306	0.256	0.0112
Bio-10_Con	UD	UD	UD	0.0267	0.0274	0.0933	0.0033	0.0048	0.0055	0.0300	0.0289	0.0124	UD	UD	UD	0.0272	0.353	0.0073
Bio-10_+7 °C	0.0210	0.0227	UD	0.0189	0.0214	0.0761	UD	0.0075	UD	0.0225	0.0157	0.0076	UD	UD	UD	0.0369	0.324	0.0101
Bio-13_Ini	0.0743	0.151	0.0686	0.0964	0.0841	0.2818	0.0104	0.0169	0.0238	0.0784	0.127	UD	0.0098	0.0077	0.0058	0.0761	0.647	0.0421
Bio-13_Con	0.0930	0.0827	UD	0.111	0.0695	0.2465	0.0068	0.0164	0.0148	0.0632	0.0658	0.0598	UD	UD	UD	0.0544	0.857	0.0241
Bio-13_+7 °C	UD	0.0440	UD	0.112	0.0638	0.2145	0.0062	0.0147	0.0127	0.0569	0.0538	0.0541	UD	UD	UD	0.0524	0.774	0.0197

Chl: chlorophyll, Chlide: chlorophilide, Peri: peridinin, 19′-BF: 19′-butanoyloxyfucoxanthin, Fuco: fucoxanthin, Neo: neoxanthin, Prasino: prasinoxanthin, Viola: violaxanthin, 19′-HF: 19′- hexanoyloxyfucxanthin, DD: diadinoxanthin, Allo: alloxanthin, DT: diatoxanthin, Zea: zeaxanthin, Lut: lutein, Caro: carotene.

Appendix C

FRRf parameters obtained at all sampling stations ± standard deviations, $n = 2$.

Station	$F_v/F_{m\ FRRf}$	σ_{PSII}	[RCII]
	–	$\times$ nm^2 PSII^{-1}	$\times 10^{-9}$ mol m^{-3}
Bio-1	0.582	2.69	0.49
Bio-2	0.322 ± 0.064	3.78 ± 0.64	1.54 ± 0.84
Bio-4	0.421 ± 0.024	2.79 ± 0.16	1.04 ± 0.20
Bio-6	0.467 ± 0.068	2.56 ± 0.19	1.50 ± 0.31
Bio-7	0.515 ± 0.064	2.85 ± 0.15	0.76 ± 0.33
Bio-9	0.394 ± 0.026	2.91 ± 0.16	1.23 ± 0.25
Bio-10	0.377 ± 0.050	3.06 ± 0.30	0.62 ± 0.11
Bio-11	0.504 ± 0.033	2.78 ± 0.14	1.24 ± 0.12
Bio-12	0.475 ± 0.049	3.01 ± 0.08	1.15 ± 0.27
Bio-13	0.432 ± 0.020	3.13 ± 0.19	1.94 ± 0.16
Bio-14	0.477 ± 0.005	2.43 ± 0.15	5.57 ± 0.22
AK15-1	ND	ND	ND
AK15-2	ND	ND	ND

F_v/F_{mFRRf}: Maximum quantum yield of PSII obtained by FRR fluorometer. σ_{PSII}: Functional absorption cross-section for PSII. [RCII]: Concentration of functional PSII reaction center.

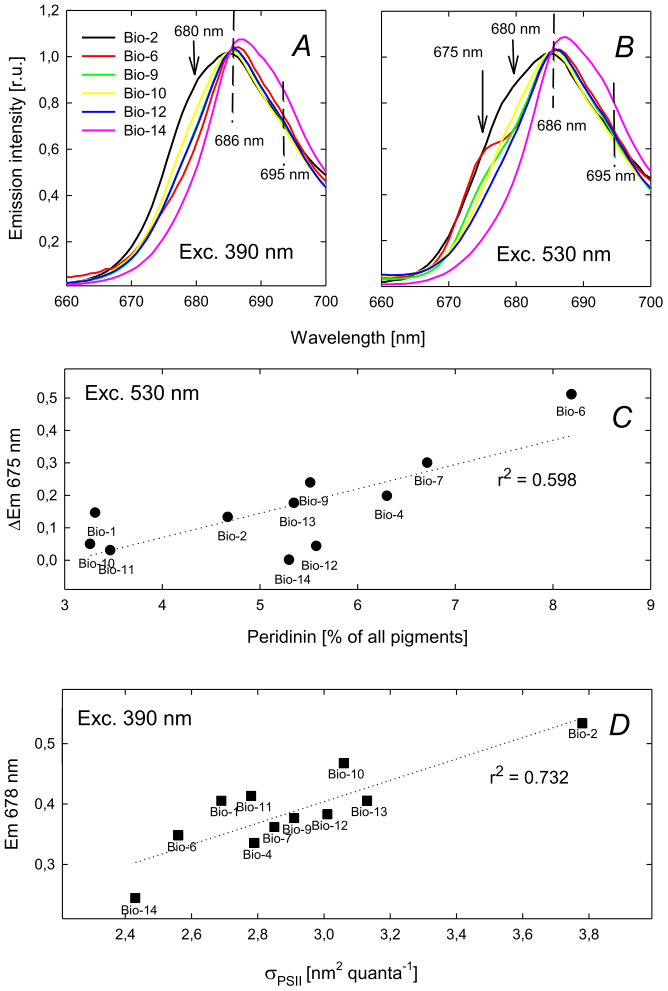

Appendix D. Low temperature (77K) emission spectra. Panels A and B show part of the emission in the range 660–700 nm of selected samples from different stations. (A) shows spectra excited by 390 nm, (B) shows spectra excited at 530 nm. The arrows and lines indicate the positions of individual emission bands (675, 680, 685, 695 nm). (C) shows relationship between the relative content of peridinin (% of all pigments) and the increase of the 675 nm emission when excited at 530 nm (calculated as difference between emission at 675 nm when excited at 530 and 390 nm). (D) shows the relationship between PSII effective cross-section (σ_{PSII}) and the emission band intensity at 678 nm when excited at 390 nm.

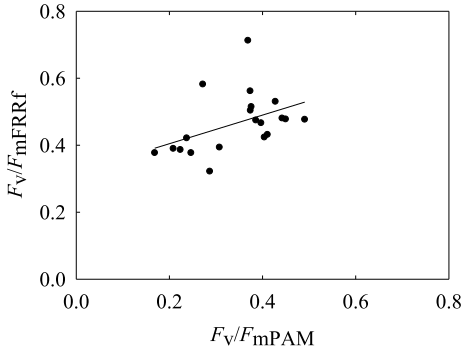

Appendix E. A relationship between F_v/F_{mPAM} and F_v/F_{mFRRf}.
The parameters were significantly correlated each other ($\rho = 0.483$, $n = 20$, $p < 0.05$, Spearman's Rank correlation).
F_v/F_{mPAM}: Maximum quantum yield of PSII obtained by PAM fluorometry.
F_v/F_{mFRRf}: Maximum quantum yield of PSII obtained by FRR fluorometry.

References

Abe, Y., Yamaguchi, A., Matsuno, K., Kono, T., Imai, I., 2014. Short-term changes in the population structure of hydromedusa *Aglantha digitale* during the spring phytoplankton bloom in the Oyashio region. Bull. Fish. Sci. Hokkaido Univ. 64, 71–81.

Babin, M., Stramski, D., 2002. Light absorption by aquatic particles in the near-infrared spectral region. Limnol. Oceanogr. 47, 911–915.

Behrenfeld, M.J., 2010. Abandoning Sverdrup's critical depth hypothesis on phytoplankton blooms. Ecology 91, 977–989.

Behrenfeld, M.J., Prasil, O., Babin, M., Bruyant, F., 2004. In search of a physiological basis for covariations in light-limited and light-saturated photosynthesis. J. Phycol. 40, 4–25.

Behrenfeld, M.J., Randerson, J.T., McClain, C.R., Feldman, G.C., Los, S.O., Tucker, C.J., Falkowski, P.G., Field, C.B., Frouin, R., Esaias, W.E., Kolber, D.D., Pollack, N.H., 2001. Biospheric primary production during an ENSO transition. Science 291, 2594–2597.

Chiba, S., Ono, T., Tadokoro, K., Midorikawa, T., Saino, T., 2004. Increased stratification and decreased lower trophic level productivity in the Oyashio Region of the North Pacific: a 30-year retrospective study. J. Oceanogr. 60, 149–162.

Cleveland, J.S., Weidemann, A.D., 1993. Quantifying absorption by aquatic particles: a multiple scattering correction for glass-fiber filters. Limnol. Oceanogr. 38, 1321–1327.

Crafts-Brandner, S.J., Salvucci, M.E., 2000. Rubisco activase constrains the photosynthetic potential of leaves at high temperature and CO_2. Proc. Natl. Acad. Sci. U. S. A 97, 13430–13435.

Descolas-Gros, C., de Billy, G., 1987. Temperature adaptation of RuBP carboxylase: kinetic properties in marine Antarctic diatoms. J. Exp. Mar. Biol. Ecol. 108, 147–158.

D'Haene, S.E., Sobotka, R., Bučinská, L., Dekker, J.P., Komenda, J., 2015. Interaction of the PsbH subunit with a chlorophyll bound to histidine 114 of CP47 is responsible for the red 77K fluorescence of Photosystem II. Biochim. Biophys. Acta 1847, 1327–1334.

Endo, H., Sugie, K., Yoshimura, T., Suzuki, K., 2015. Effects of CO_2 and iron availability on *rbcL* gene expression in Bering Sea diatoms. Biogeosciences 12, 2247–2259.

Endo, H., Sugie, K., Yoshimura, T., Suzuki, K., 2016. Response of spring diatoms to CO_2 availability in the western North Pacific as determined by next-generation sequencing. PLoS One 11 e0154291.

Endo, H., Yoshimura, T., Kataoka, T., Suzuki, K., 2013. Effects of CO_2 and iron availability on phytoplankton and eubacterial community compositions in the northwest subarctic Pacific. J. Exp. Mar. Biol. Ecol. 439, 160–175.

Eppley, R.W., 1972. Temperature and phytoplankton growth in the sea. Fish. Bull. 70, 1063–1085.

Falkowski, P.G., 1994. The role of phytoplankton photosynthesis in global biogeochemical cycles. Photosynth. Res. 39, 235–258.

Field, C.B., Behrenfeld, M.J., Randerson, J.T., Falkowski, P.G., 1998. Primary production of the biosphere: integrating terrestrial and oceanic components. Science 281, 237–240.

Hama, T., Miyazaki, T., Ogawa, Y., Iwakuma, T., Takahashi, M., Otsuki, A., Ichimura, S., 1983. Measurement of photosynthetic production of a marine phytoplankton population using a stable ^{13}C isotope. Mar. Biol. 73, 31–36.

Hasle, G.R., Syvertsen, E.E., 1996. Marine diatoms. In: Tomas, C.R. (Ed.), Identifying Marine Phytoplankton. Academic Press, San Diego, pp. 5–386.

Hattori-Saito, A., Nishioka, J., Ono, T., McKay, R.M.L., Suzuki, K., 2010. Iron deficiency in micro-sized diatoms in the Oyashio region of the western subarctic Pacific during spring. J. Oceanogr. 66, 105–115.

Hill, R., Larkum, A.W.D., Prášil, O., Kramer, D.M., Szabó, M., Kumar, V., Ralph, P.J., 2012. Light-induced dissociation of antenna complexes in the symbionts of scleractinian corals correlates with sensitivity to coral bleaching. Coral Reefs 31, 963–975.

Honda, M.C., 2003. Biological pump in northwestern North Pacific. J. Oceanogr. 59, 671–684.

Hooker, S.B., Morrow, J.H., Matsuoka, A., 2013. Apparent optical properties of the Canadian Beaufort Sea – Part 2: the 1 % and 1 cm perspective in deriving and validating AOP data products. Biogeosciences 10, 4511–4527.

Hooker, S.B., 2014. Mobilization protocols for hybrid sensors for environmental AOP sampling (HySEAS) observations. In: NASA Tech. Pub. NASA Goddard Space Flight Center, Greenbelt, Maryland, pp. 105 2014 – 217518.

Ikeda, T., Shiga, N., Yamaguchi, A., 2008. Structure, biomass distribution and trophodynamics of the pelagic ecosystem in the Oyashio region, western subarctic Pacific. J. Oceanogr. 64, 339–354.

Isada, T., Hattori-Saito, A., Saito, H., Ikeda, T., Suzuki, K., 2010. Primary productivity and its bio-optical modeling in the Oyashio region, NW Pacific during the spring bloom 2007. Deep-Sea Res. II 57, 1653–1664.

Isada, T., Iida, T., Liu, H., Saitoh, S.I., Nishioka, J., Nakatsuka, T., Suzuki, K., 2013. Influence of Amur River discharge on phytoplankton photophysiology in the Sea of Okhotsk during late summer. J. Geophys. Res. Ocean 118, 1995–2013.

Isada, T., Kuwata, A., Saito, H., Ono, T., Ishii, M., Yoshikawa-Inoue, H., Suzuki, K., 2009. Photosynthetic features and primary productivity of phytoplankton in the Oyashio and Kuroshio–Oyashio transition regions of the northwest Pacific. J. Plankton Res. 31, 1009–1025.

Isoda, Y., Kishi, M.J., 2003. A summary of "coastal Oyashio" symposium (in Japanese). Bull. Coast. Oceanogr 41, 1–3.

John, D.E., Patterson, S.S., Paul, J.H., 2007. Phytoplankton-group specific quantitative polymerase chain reaction assays for RuBisCO mRNA transcripts in seawater. Mar. Biotechnol. 9, 747–759.

Kasai, H., Saito, H., Yoshimori, A., Taguchi, S., 1997. Variability in timing and magnitude of spring bloom in the Oyashio region, the western subarctic Pacific off Hokkaido. Japan. Fish. Oceanogr 6, 118–129.

Kawakami, H., Honda, M.C., Matsumoto, K., Wakita, M., Kitamura, M., Fujiki, T., Watanabe, S., 2015. POC fluxes estimated from ^{234}Th in late spring–early summer in the western subarctic North Pacific. J. Oceanogr. 71, 311–324.

Kawakami, H., Yang, Y.L., Honda, M.C., Kusakabe, M., 2004. Particulate organic carbon fluxes estimated from ^{234}Th deficiency in winters and springs in the northwestern North Pacific. Geochem. J. 38, 581–592.

Kiefer, D.A., Reynolds, R.A., 1992. Advances in understanding phytoplankton fluorescence and photosynthesis. In: Falkowski, P.G., Woodhead, A.D. (Eds.), Primary Productivity and Biogeochemical Cycles in the Sea. Springer Science & Business Media, New York, pp. 155–174.

Kirk, J.T.O. (Ed.), 2010. Light and Photosynthesis in Aquatic Ecosystems, third ed. Cambridge Univ. Press, New York, pp. 622.

Kishino, M., Takahashi, M., Okami, N., Ichimura, S., 1985. Estimation of the spectral absorption coefficients of phytoplankton in the sea. Bull. Mar. Sci. 37, 634–642.

Kolber, Z., Falkowski, P.G., 1993. Use of active fluorescence to estimate phytoplankton photosynthesis in situ. Limnol. Oceanogr. 38, 1646–1665.

Kolber, Z., Prášil, O., Falkowski, P.G., 1998. Measurements of variable chlorophyll fluorescence using fast repetition rate techniques: defining methodology and experimental protocols. Biochim. Biophys. Acta 1367, 88–106.

Kono, T., 1997. Modification of the Oyashio water in the Hokkaido and tohoku areas. Deep-Sea Res. I 44, 669–688.

Kono, T., Foreman, M., Chandler, P., Kashiwai, M., 2004. Coastal Oyashio south of Hokkaido. Japan. J. Phys. Oceanogr 34, 1477–1494.

Kono, T., Sato, M., 2010. A mixing analysis of surface water in the Oyashio region: its implications and application to variations of the spring bloom. Deep-Sea Res. II 57, 1595–1607.

Kusaka, A., Azumaya, T., Kawasaki, Y., 2013. Monthly variations of hydrographic structures and water mass distribution off the Doto area. Japan. J. Oceanogr 69, 295–312.

Li, W.K.W., Smith, J., Platt, T., 1984. Temperature response of photosynthetic capacity and carboxylase activity in Arctic marine phytoplankton. Mar. Ecol. Prog. Ser 17, 237–243.

Liu, H., Suzuki, K., Nishioka, J., Sohrin, R., Nakatsuka, T., 2009. Phytoplankton growth and microzooplankton grazing in the Sea of Okhotsk during late summer of 2006. Deep-Sea Res. I 56, 561–570.

MacIntyre, H.L., Kana, T.M., Anning, T., Geider, R.J., 2002. Photoacclimation of photosynthesis irradiance response curves and photosynthetic pigments in microalgae and cyanobacteria. J. Phycol. 38, 17–38.
McQuoid, M.R., Godhe, A., 2004. Recruitment of coastal planktonic diatoms from benthic versus pelagic cells: variations in bloom development and species composition. Limnol. Oceanogr. 49, 1123–1133.
Mochizuki, M., Shiga, N., Saito, M., Imai, K., Nojiri, Y., 2002. Seasonal changes in nutrients, chlorophyll *a* and the phytoplankton assemblage of the western subarctic gyre in the Pacific Ocean. Deep-Sea Res. II 49, 5421–5439.
Mock, T., Hoch, N., 2005. Long-term temperature acclimation of photosynthesis in steady-state cultures of the polar diatom *Fragilariopsis cylindrus*. Photosynth. Res. 85, 307–317.
Monterey, G., Levitus, S., 1997. Seasonal variability of mixed layer depth for the world ocean. NOAA Atlas NESDIS 14, 100.
Nishimura, A., Hamatsu, T., Yabuki, K., Shida, O., 2002. Recruitment fluctuations and biological responses of walleye pollock in the Pacific coast of Hokkaido. Fish. Sci. 68, 206–209.
Obayashi, Y., Tanoue, E., Suzuki, K., Handa, N., Nojiri, Y., Wong, C.S., 2001. Spatial and temporal variabilities of phytoplankton community structure in the northern North Pacific as determined by phytoplankton pigments. Deep-Sea Res. I 48, 439–469.
Ogasawara, J., 1990. Physics on the east and south coasts of Hokkaido (in Japanese). In: Kunishi, H. (Ed.), Coastal Oceanography of Japanese Islands. Tokai University Press, pp. 839.
Oguma, S., Ono, T., Kusaka, A., Kasai, H., Kawasaki, Y., Azumaya, T., 2008. Isotopic tracers for water masses in the coastal region of Eastern Hokkaido. J. Oceanogr. 64, 525–539.
Ohtani, K., 1971. Studies on the change of the hydrographic conditions in the Funka bay PartII: characteristics of the waters occupying the Funka bay (in Japanese with English abstract). Bull. Fac. Fish. Hokkaido Univ. 22, 58–61.
Okamoto, S., Hirawake, T., Saitoh, S.-I., 2010. Interannual variability in the magnitude and timing of the spring bloom in the Oyashio region. Deep-Sea Res. II 57, 1608–1617.
Oxborough, K., Moore, C.M., Suggett, D.J., Lawson, T., Chan, H.G., Geider, R.J., 2012. Direct estimation of functional PSII reaction center concentration and PSII electron flux on a volume basis: a new approach to the analysis to Fast Repetition Rate fluorometry (FRRf) data. Limnol Oceanogr. Meth. 10, 142–154.
Palmisano, A.C., SooHoo, J.B., Sullivan, C.W., 1987. Effects of four environmental variables on photosynthesis-irradiance relationships in Antarctic sea-ice microalgae. Mar. Biol. 94, 299–306.
Platt, T., Gallegos, C.L., Harrison, W.G., 1980. Photoinibition of photosynthesis in natural assemblages of marine phytoplankton. J. Mar. Res. 38, 103–111.
Platt, T., Jassby, A.D., 1976. The relationship between photosynthesis and light for natural assemblages of coastal marine phytoplankton. J. Phycol. 12, 421–430.
Prášil, O., Bína, D., Medová, H., Řeháková, K., Zapomělová, E., Veselá, J., Oren, E., 2009. Emission spectroscopy and kinetic fluorometry studies of phototrophic microbial communities along a salinity gradient in solar saltern evaporation ponds of Eilat. Israel. Aquat. Microb. Ecol 56, 285–296.
Ralph, P.J., McMinn, A., Ryan, K.G., Ashworth, C., 2005. Short-term effect of temperature on the photokinetics of microalgae from the surface layers of Antarctic pack ice. J. Phycol. 41, 763–769.
Raven, J.A., Geider, R.J., 1988. Temperature and algal growth. New Phytol. 110, 441–461.
Saito, H., Tsuda, A., 2003. Influence of light intensity on diatom physiology and nutrient dynamics in the Oyashio region. Prog. Oceanogr. 57, 251–263.
Saito, H., Tsuda, A., Kasai, H., 2002. Nutrient and plankton dynamics in the Oyashio region of the western subarctic Pacific Ocean. Deep-Sea Res. II 49, 5463–5486.
Sakshaug, E., Bricaud, A., Dandonneau, Y., Falkowski, P.G., Kiefer, D.A., Legendre, L., Morel, A., Parslow, J., Takahashi, M., 1997. Parameters of photosynthesis: definitions, theory and interpretation of results. J. Plankton Res. 19, 1637–1670.
Sakurai, Y., 2007. An overview of the Oyashio ecosystem. Deep-Sea Res. II 2526–2542.
Sarmiento, J.L., Siegenthaler, U., 1992. New production and the global carbon cycle. In: Falkowski, P.G., Woodhead, A.D. (Eds.), Primary Productivity and Biogeochemical Cycles in the Sea. Springer Science & Business Media, New York, pp. 317–332.
Schloss, P.D., Westcott, S.L., Ryabin, T., Hall, J.R., Hartmann, M., Hollister, E.B., Lesniewski, R.A., Oakley, B.B., Parks, D.H., Robinson, C.J., Sahl, J.W., Stres, B., Thallinger, G.G., Van Horn, D.J., Weber, C.F., 2009. Introducing mothur: open-source, platform-independent, community-supported software for describing and comparing microbial communities. Appl. Environ. Microbiol. 75, 7537–7541.
Shinada, A., Shiga, N., Ban, S., 1999. Structure and magnitude of diatom spring bloom in Funka Bay, southwestern Hokkaido, Japan, as influenced by the intrusion of Coastal Oyashio Water. Plankton Biol. Ecol. 46, 24–29.
Smetacek, V., 1999. Diatoms and the ocean carbon cycle. Protist 150, 25–32.
Suggett, D.J., Stambler, N., Prášil, O., Kolber, Z., Quigg, A., Vázquez-Dominguez, E., Zohary, T., Berman, T., Iluz, D., Levitan, O., Lawson, T., Meeder, E., Lazar, B., Bar-Zeev, E., Medova, H., Berman-Frank, I., 2009. Nitrogen and phosphorus limitation of oceanic microbial growth during spring in the Gulf of Aqaba. Aquat. Microb. Ecol. 56, 227–239.
Sugiura, J., 1956. A note on current branches in the Oyashio area (in Japanese with English abstract). J. Oceanogr. Soc. Jpn. 12, 117–119.
Suzuki, K., Handa, N., Nishida, T., Wong, C.S., 1997. Estimation of phytoplankton succession in a fertilized mesocosm during summer using high-performance liquid chromatographic analysis of pigments. J. Exp. Mar. Biol. Ecol. 214, 1–17.
Suzuki, K., Kamimura, A., Hooker, S.B., 2015. Rapid and highly sensitive analysis of chlorophylls and carotenoids from marine phytoplankton using ultra-high performance liquid chromatography (UHPLC) with the first derivative spectrum chromatogram (FDSC) technique. Mar. Chem. 176, 96–109.
Suzuki, K., Kuwata, A., Yoshie, N., Shibata, A., Kawanobe, K., Saito, H., 2011. Population dynamics of phytoplankton, heterotrophic bacteria, and viruses during the spring bloom in the western subarctic Pacific. Deep-Res. I 58, 575–589.
Suzuki, K., Liu, H., Saino, T., Obata, H., Takano, M., Okamura, K., Sohrin, Y., Fujishima, Y., 2002. East-west gradients in the photosynthetic potential of phytoplankton and iron concentration in the subarctic Pacific Ocean during early summer. Limnol. Oceanogr. 47, 1581–1594.
Suzuki, R., Ishimaru, T., 1990. An improved method for the determination of phytoplankton chlorophyll using N, N-dimethylformamide. J. Oceanogr. Soc. Jpn. 46, 190–194.
Takahashi, T., Sutherland, S.C., Sweeney, C., Poisson, A., Metzl, N., Tilbrook, B., Bates, N., Wanninkhof, R., Feely, R.A., Sabine, C., Olafsson, J., Nojiri, Y., 2002. Global sea-air CO_2 flux based on climatological surface ocean pCO_2, and seasonal biological and temperature effects. Deep-Sea Res. II 49, 1601–1622.
Taniguchi, A., 1999. Differences in the structure of the lower trophic levels of pelagic ecosystems in the eastern and western subarctic Pacific. Prog. Oceanogr. 43, 289–315.
Van Heukelem, L., Thomas, C.S., 2001. Computer-assisted high-performance liquid chromatography method development with applications to the isolation and analysis of phytoplankton pigments. J. Chromatogr. A 910, 31–49.
Verity, P.G., 1981. Effects of temperature, irradiance, and daylength on the marine diatom *Leptocylindrus danicus* Cleve. I. Photosynthesis and cellular composition. J. Exp. Mar. Biol. Ecol. 55, 79–91.
Welschmeyer, N.A., 1994. Fluorometric analysis of chlorophyll *a* in the presence of chlorophyll *b* and pheopigments. Limnol. Oceanogr. 39, 1985–1992.
Yamaguchi, A., Miwa, Y., Inoue, K., Matsumoto, T., 2003. Characteristics of zooplankton community in the coastal Oyahsio water (in Japanese with English abstract). Bull. Coast. Oceanogr 41, 23–31.
Yasuda, I., 2003. Hydrographic structure and variability in the Kuroshio-Oyashio transition area. J. Oceanogr. 59, 389–402.
Yoshie, N., Suzuki, K., Kuwata, A., Nishioka, J., Saito, H., 2010. Temporal and spatial variations in photosynthetic physiology of diatoms during the spring bloom in the western subarctic Pacific. Mar. Ecol. Prog. Ser 399, 39–52.
Yoshie, N., Yamanaka, Y., Kishi, M.J., Saito, H., 2003. One dimensional ecosystem model simulation of the effects of vertical dilution by the winter mixing on the spring diatom bloom. J. Oceanogr. 59, 563–571.
Yoshimori, A., Ishizaka, J., Kono, T., Kasai, H., Saito, H., Kishi, M.J., Taguchi, S., 1995. Modeling of spring bloom in the western subarctic Pacific (off Japan) with observed vertical density structure. J. Oceanogr. 51, 471–488.
Young, J.N., Goldman, J.A.L., Kranz, S.A., Tortell, P.D., Morel, F.M.M., 2015. Slow carboxylation of Rubisco constrains the rate of carbon fixation during Antarctic phytoplankton blooms. New Phytol. 205, 172–181.